Energy Conversion and Management 284 (2023) 116973

Contents lists available at ScienceDirect

Energy Conversion and Management

journal homepage: www.elsevier.com/locate/enconman

Coupling an oxygen generation cycle with an oxy-fuel combustion spark ignition engine for zero NOx emissions and carbon capture: A feasibility study

José Ramón Serrano, Francisco José Arnau, Luis Miguel García-Cuevas *, Fabio Alberto Gutiérrez

CMT – Motores Térmicos. Universitat Politècnica de València. Camino de Vera s/n, Valencia, 46022, Valencia, Spain

ARTICLE INFO

Keywords:
Oxy-fuel combustion
O_2 production
Membrane
Engine

ABSTRACT

An oxycombustion spark-ignition engine coupled to an O_2 production cycle based on a mixed electronic-ionic ceramic-type membrane is studied in this paper. The exhaust gases drive oxygen production through a heat exchanger network and a set of turbochargers. Initially, a study at medium speed is carried out to determine the influence of the oxygen concentration and the engine compression ratio on the system performance. A 16.3 % of fuel consumption reduction is reached when 30 % of O_2 mass fraction and an engine compression ratio of 20 are implemented when compared with conventional engine operation. Then, a full load study in a wide range of engine speeds is performed, where a maximum fuel consumption reduction of 21 % is obtained at high speed (5000 rpm) comparing with conventional engine operation. The study shows the whole cycle has demonstrated promising performance parameters at different working conditions (O_2 mass fraction, compression ratio, engine load and speed).

1. Introduction

The different regulations related to automobile pollutants and greenhouse gas emissions have generated efforts in different spheres to develop technologies that allow the imposed standards. In the European Union (EU) exists the 2030 climate and energy framework, whose key targets are to reduce by 40% the greenhouse gas emissions compared with the 1990 levels, have a 32% share of renewable energies and improve by 32.5% the energy efficiency of the European industry [1]. This framework was proposed according to the international commitments in the Paris Agreement, formally ratified in 2016 by the EU [2].

In this sense, some standards, such as the European standard emissions (EURO standards), appear to gradually reduce the emissions of the new vehicles sold in the UE territory. In Table 1, it is seen the proposed limits for the last European regulation (EURO 7) for pollutant emissions in engines, released in November 2022.

In this context, different strategies to reduce the produced pollution by vehicles have been studied, among which oxycombustion is found to be one of the most promising alternatives to be applied. Oxycombustion consists of burning fuel in an atmosphere of oxygen combined with recycled exhaust gases to control the combustion temperature, which changes the typical combustion process of air, eliminating N_2 from the reaction [3].

According to [4], two main benefits of oxycombustion can be applicable when applied in vehicle engines: First, the heat losses are reduced due to the elimination of bulk N_2 that is heated up during the combustion and cooled down at the exhaust. Since only recycled gas is used to control the combustion temperature, the mass of flue gases is reduced, decreasing the heat losses. Second, a near-zero emission system can be achieved. By eliminating N_2 from the combustion process, the presence of NO_x in the exhaust gases is almost eliminated. Also, a CO_2/H_2O composition of exhaust gases is obtained, where water could be condensed for CO_2 sequestration.

In internal combustion engines, oxycombustion has been studied in diesel and gasoline engines of different sizes and applications. Operating parameters such as oxygen and exhaust gas recirculation (EGR) concentration, water injection, compression ratio, or supplement fuels are varied to achieve a good engine performance with low emissions.

In the study performed by Wu et al. [5], a 125 cm^3 single-cylinder spark-ignition engine is studied under oxycombustion with different EGR concentrations and water injection. The compression ratio is 9.2, and the fuel used is propane. A maximum efficiency increase of 9.4 % (32.1 % to 41.5 %) is achieved. Thermal efficiency decreases only when high amounts of water and relatively high EGR concentrations are implemented because flame propagation is affected. Also, water injection temperature is important due to the reduction of the extracted energy for evaporation.

The HCCI mode under oxycombustion is studied by Kang et al. [6], where an 800 cm^3 single-cylinder engine is used, with a compression

* Corresponding author.
E-mail address: luiga12@mot.upv.es (L.M. García-Cuevas).
URL: https://www.cmt.upv.es/ (L.M. García-Cuevas).

https://doi.org/10.1016/j.enconman.2023.116973
Received 21 December 2022; Received in revised form 24 March 2023; Accepted 26 March 2023
Available online 1 April 2023

Table 1
Regulation Euro 7 for engines. Maximum allowed values for certain pollutants [7].

	Light duty
NO_x [g km^{-1}]	0.060
PM [g km^{-1}]	0.0045
CO [g km^{-1}]	0.500
HC [g km^{-1}]	0.100
	Heavy duty
NO_x [g kW^{-1} h^{-1}]	0.090
PM [g kW^{-1} h^{-1}]	0.008
CO [g kW^{-1} h^{-1}]	0.200
HC [g kW^{-1} h^{-1}]	0.400

ratio of 17 and n-heptane as fuel. At these conditions, the CO_2 addition in the combustion reaction significantly impacts the process due to its higher specific heat ratio compared with air and the limitation of flame propagation. In the study, using 15 % of CO_2 extends the combustion duration in 11° compared with using pure oxygen and 8° when compared with conventional combustion. It was also found that water injection at high temperatures and pressure can control abnormal combustion and improve thermal efficiency.

A four-cylinder compression ignition engine with a compression ratio of 17 and using diesel as fuel is studied in Tan et al. [8]. The engine is tested at 600 rpm to 800 rpm at idling and part-load conditions. Different combinations of oxygen, nitrogen, and carbon dioxide are implemented as working gas for combustion. The authors found that increasing the oxygen concentration contributes to improving the combustion efficiency and increasing the total emissions. However, when the engine uses an O_2/CO_2 atmosphere, NO_x emissions are eliminated, with the benefits of a high combustion efficiency as oxygen concentration increases.

Oxycombustion mode was examined by Van Blarigan et al. [9] using a spark ignition engine with a compression ratio of 17, where an optimal oxygen concentration was determined. Maximum thermal efficiency of 24.2% is achieved, which is 7.2% lower when compared with the conventional operation. This difference is explained due to the reduced ratio of specific heats of the working gas when oxycombustion is implemented.

A HCCI engine under different O_2/CO_2 proportions at the intake and considering distinct load levels is studied by Mobasheri et al. [10]. A 4-cylinder 4-stroke diesel engine of 2000 cm^3 and a compression ratio of 18.2 is used, operating at 2000 rpm. Here, the volumetric oxygen concentration varies from 17 % to 23 % at different fuel-injected amounts. Higher oxygen concentrations help shorten the ignition period and the combustion duration, resulting in a higher temperature and pressure in the cylinder. In this case, an increase of thermal efficiency of 11.8 % is achieved when the O_2 concentration is increased from 17 % to 23 % at low loads.

Regarding water injection, Yu et al. [11] studied an internal combustion rankine cycle (ICRC), an oxycombustion engine with water injection at the cylinders. An oxygen/carbon dioxide mixture is the working gas, setting the oxygen concentration at 40 %. Optimizing variables such as water mass flow and injection timing and pressure, an enhancement of 7.8 % is obtained in indicated work. On the other hand, Wu et al. [12] performed a similar study in an ICRC using a 125 cm^3 SI single-cylinder engine fueled with propane. When water injection is considered, an increase of 23 % is achieved.

The effect of the compression ratio on an engine performance under oxycombustion mode is studied by Gao et al. [13] under similar conditions used in the works of Wu et al. [5,12], emphasizing in the compression ratio effect. As it is expected, increasing the compression ratio (from 9.2 to 14 in this study) improves the engine thermal efficiency by 4.9 %. However, when water is injected, the mass increment during the expansion and the reduction of the in-cylinder gas heat capacity helps increase the engine performance even to 22.4 %, as the tendency of knocking is avoided due to decreasing the flame propagation and in-cylinder temperature.

On the other hand, Wu et al. [14] examined ethanol and gasoline as fuel supplements in a diesel engine, in which oxycombustion is implemented for pollutant gas reduction. Different conditions are studied, finding that adding both supplementary fuels is beneficial to reduce NO_x, CO_2, and smoke emissions. No information about the effects of fuel consumption is found in the publication.

However, these studies show that the oxygen source for combustion is pressurized bottles, increasing the costs of applying oxycombustion technology if applied in conventional vehicles. Considering this, oxygen production in situ during the vehicle operation is required, allowing an autonomous system in oxycombustion mode. In other words, a method for air separation is demanded, where high-purity oxygen is obtained to be mixed with EGR and driven into the engine intake.

Currently, the most feasible method for air separation is Cryogenic Air Separation (CAS), where fractional distillation of air at low temperature and pressure is performed, and the different air components are separated according to their boiling temperature [15]. However, it is a highly energy-intensive separation method whose energy consumption could represent between 10 % to 40 % of the gross output in an oxy-fuel combustion plant. Also, it requires a multi-column process with air compression, which implies a significant amount of mass and volume that is not feasible in automobile applications [15].

Considering this, mixed ionic-electronic conducting (MIEC) membranes arise as a promising method for air separation in oxy-fuel combustion applications. MIEC membranes are a type of dense membranes in which oxygen ions are diffused through the membrane via lattice vacancies or interstitial sites under an oxygen chemical potential gradient across the membrane, achieved when the operating conditions are high temperatures (700 °C to 1000 °C) and gradient pressures (1-2 MPa at feed side, vacuum pressure at permeate side) [16]. Compared with CAS, this technology has an oxygen selectivity of 100%, lower energy consumption, less initial investment, and is easily integrated into industrial processes [16].

MIEC membranes for oxygen production have been studied in applications concerning oxycombustion for power plants and industrial processes [17–19], where the energy penalty for using CAS is reduced as it is replaced by membrane-based oxygen production. For example, Portillo et al. [19] studied the performance of a power plant with a gross output of 860 MW, where the conventional operation is compared with the oxycombustion mode considering two alternatives of oxygen production, cryogenic and MIEC membranes. Compared with the conventional operation, a 7.6 % of net thermal efficiency is reduced when the cryogenic method is used, while a 2.5 % reduction when the best membrane case is evaluated, demonstrating a better energy performance.

Regarding MIEC membrane application for oxygen production in engines, there are a couple of studies regarding coupling a membrane-based cycle for oxygen production to an engine for oxy-fuel combustion operation. Serrano et al. [20] studied the feasibility of coupling an oxygen production cycle to a 2.2 l, compression ignition engine where two different EGR control systems are assessed. When compared at high engine speeds with the conventional operation, the proposed engine configurations for oxy-fuel combustion exhibit similar brake power and indicated efficiencies, while higher differences for fuel consumption are found for low speeds (more than 10 % for oxy-fuel configuration) but reaching an increase of 30 % for brake power. Additionally, it is worth mentioning that this configuration is suitable for CO_2 capture, according to the authors.

On the other hand, Novella et al. [21] studied a 1.3 l spark-ignition engine coupled with a membrane-based oxygen production cycle, comparing its performance with the conventional operation of that engine. For the same brake power, the oxycombustion mode performs better at high speeds because of the increasing equivalence ratio in conventional operation to reduce the exhaust temperature and protect

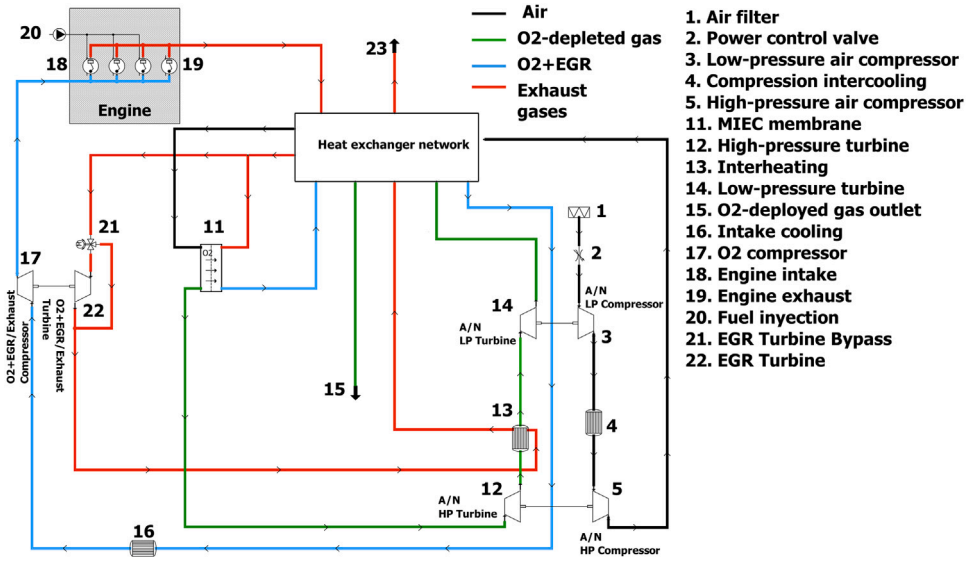

Fig. 1. Spark ignition engine working by oxy-fuel combustion means and in situ oxygen production.

the turbogroup integrity. This additional fuel is not necessary under oxycombustion mode due to the presence of heat exchangers that assure acceptable temperatures for these elements. It was also found that 50% of the burnt fuel energy is recovered in the heat exchanger network and turbochargers for oxygen production at the membrane. The paper also concludes with the proposal of increasing the compression ratio before detonation, finding it an attractive method to improve performance.

This paper evaluates the effect of the oxygen concentration at the intake and the compression ratio of the cylinders in a spark-ignition engine working under oxy-fuel combustion with oxygen production in situ using a MIEC-type membrane. The motivation of this work is to test the feasibility of operating a reciprocating engine using gasoline as fuel but with zero tailpipe emissions, which is expected to have clear advantages against other alternatives, such as battery-electric powerplants, in terms of the overall specific energy of the system. The authors considered a similar heat exchanger network as the one proposed in Serrano et al. [20] to increase air stream temperature to feed the membrane, where the thermal energy of different gas flows within the system is exploited.

First, this study examines the influence of the oxygen mass fraction at the intake and the compression ratio at medium engine speed as reference. Several variables are considered for the analysis, such as the brake-specific fuel consumption (BSFC), the temperature at the exhaust manifold, cylinder pressure and temperature and turbomachines performance, explaining its variation in terms of the combustion nature, in-cylinder variables and the controllable variables as turbine and valves openings.

This parametric evaluation works as a proof of concept, where the different oxygen concentrations and compression ratios are assessed to determine its operative viability. Both parameters are modified due to lacking criteria to acknowledge the correct direction for designing a feasible system. It is possible that some oxygen concentrations are not viable in terms of fuel consumption, engine integrity, or energy availability to operate oxygen production. Conversely, as a different type of combustion is presented, the compression ratio selection could not be the same as for conventional operation.

Then, the optimum conditions for oxygen concentration and compression ratio are used to study the behavior of the system in a wide range of engine speeds, comparing its performance with the conventional operation. The final objective is to demonstrate whether the system is feasible in terms of performance and energy efficiency, as well as in the integrity of the system components, which are critical for propulsion systems.

2. System description

The configuration of the studied system is shown in Fig. 1, which consists of the coupling of two different cycles working together to operate the engine in oxycombustion mode. This design is based on the patent described in Arnau et al. [22]. First, there is a modified Brayton cycle, which is used to produce a nitrogen-free oxygen stream. In this cycle, atmospheric air is driven by two intercooled stages of compressors (3 and 5). Then, the air goes into a series of heat exchangers to recover thermal energy from different streams of the system: First, the air flow is split into two streams to recover energy in 6 and 7 (Fig. 2) from cold exhaust gases and O_2/EGR gases respectively; then, the air is rejoined and heated up in 8 (Fig. 2) by hot oxygen-depleted gas that comes from the membrane; finally, it exchanges energy with hot O_2/EGR and exhaust gases in 9 and 10 (Fig. 2). After all of these heat-exchanging processes, the air goes into the membrane with high temperature and pressure conditions for the optimum performance of the MIEC membrane.

In the membrane (11 at (Fig. 1)), there is a mass exchange where the amount of oxygen in the air of the feed side is reduced, leaving an oxygen-depleted gas composed mainly of nitrogen and residual oxygen. This stream is also at high temperature and pressure conditions, which is used as an energy source for two expansion stages (12 and 14 at (Fig. 1)) that drive the air compressors and, finally, heat the air in 8 (Fig. 2).

On the other hand, (Fig. 1) shows a power cycle that consists of a spark-ignition engine whose exhaust gases are firstly used in 10 (Fig. 2), a high-temperature heat exchanger, and then they are split into two parts: First, there is a part of these exhaust gases that goes through a turbine (22). This turbine controls the amount of EGR that is moved to sweep the membrane on its permeate side (and the oxygen mass fraction at the engine intake as a consequence) by changing its opening: When the turbine is more open, more exhaust gases go through the turbine, leaving less mass flow to the permeate side of the stream division. The outlet turbine gases are finally used to take advantage of its high temperature by increasing the air temperature in 6 (Fig. 2) and reheating the oxygen-depleted gas between the two expansion stages in 13. The other part of the exhaust gases is used to sweep the membrane to reduce the oxygen partial pressure on the permeate side.

In the membrane, the exhaust gases stream obtains oxygen in a mass exchange with the atmospheric air on the feed side, leaving a high-temperature gas composed of carbon dioxide, water vapor, and oxygen (O_2/EGR gas). To take advantage of this energy and to reduce the

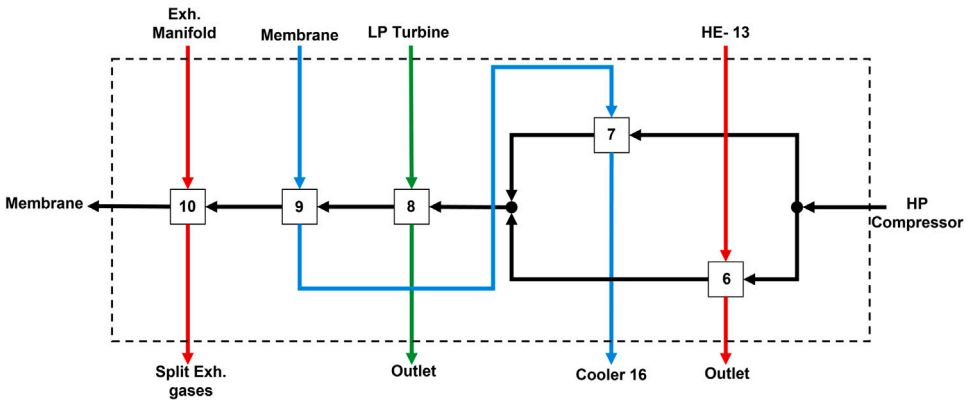

Fig. 2. Heat exchanger network adapted from the work by Serrano et al. [20].

gas temperature that will finally go to the intake engine, the O_2/EGR gas heat up the air in a high and low-temperature heat exchanger (9 and 7, respectively, as shown in Fig. 2) to be cooled in 16 (Fig. 1) to assure a temperature of 85 °C at the intake, avoiding significant amounts of liquid water at the intake. Then, the O_2/EGR gas goes through a compressor driven by element 22, considering potential energy recovering to increase the gas density and, therefore, the engine volumetric efficiency. Finally, the O_2/EGR gas comes into the engine to react with the fuel in an Otto cycle, completing the cycle of the engine part of the system.

3. Methodology

The effect of different oxygen concentrations and the compression ratio of the cylinder is studied in an oxycombustion engine with oxygen production in situ by membrane means. Oxygen mass fractions at the intake between 28%–32% are examined, while the compression ratio of the cylinders is varied between 9.6–20. These oxygen concentration ranges are selected due to the findings made in the studies by Serrano et al. [23,24]. They reported that EGR (mainly CO_2) concentration limits the engine operation due to its effects on combustion stability and flame temperature, finding EGR intake concentrations limits between 67% to 75%. Lower values than 67% generate thermal risks in the combustion chamber and the exhaust line, while higher values than 75% lead to combustion instabilities. For this reason, this study has a limited oxygen concentration (and EGR as a consequence). The effect of replacing N_2 with CO_2 as a bulk gas will be further explained in Section 4.2.1. On the other hand, for the evaluated compression ratio range, the CFD methodology from the studies mentioned above has been validated with their experimental campaign performed firstly and then used to demonstrate that a superior limit of 20 is found for knocking appearance, using these results to adjust the used combustion models in the present paper.

The baseline is obtained using a 1.3 L turbocharged and direct-injection spark-ignition engine, modeled and experimentally studied while operating in conventional mode. For oxycombustion mode modeling, a 0D/1D software called VEMOD (Virtual Engine Modeling) [25] is used considering realistic combustion laws where EGR effects are considered. Additionally, some assumptions, simplifications, and limitations are considered in this study.

3.1. Engine specification and benchmarking

In Table 2 are enlisted the specifications of the studied engine. First, the conventional mode performance of the engine is obtained by Serrano et al. [26] where a methodology to analyze the impact on the performance of spark-ignition engines of variable geometry turbine technology, assessing the full load performance of the engine, obtaining torque and brake specific fuel consumption data. These experimental data are considered a baseline, where the simulations aim for the same power value for each studied engine speed in oxycombustion mode.

Table 2
Specifications of the studied engine.

Type	4-cylinder 4-stroke spark ignition
Valves per cylinder	4
Bore [mm]	72.2
Stroke [mm]	81.35
Compression ratio [-]	9.6
Displacement [cm^3]	1332
Connecting rod length [mm]	128.128

Table 3
Fuel characteristics used in the study.

Type	Gasoline
Formula	$CH_{1.992}O_{0.016}$
Heat value MJ kg^{-1}	42.399
Density kg m^{-3}	730.3

Additionally, the reference fuel characteristics used by Serrano et al. [26] and in the present study are enlisted in Table 3.

3.2. Computational tool and implemented models

A software developed in CMT–Motores Térmicos called VEMOD (Virtual Engine Modeling) [25] is used to do the calculations in this study. This is a 0D/1D modeling software that was primarily developed to assess engines but could currently be used to model different industrial cycles. VEMOD has been used successfully to calculate energy flow in engines, as well as thermodynamic conditions in several studies as found in Olmeda et al. [27], Serrano et al. [20] or Arnau et al. [28].

For this engine operating in oxycombustion mode, submodels of coolers, heat exchangers, pipes and engine cylinders are implemented, as well as turbochargers calculations and combustion laws. Energy and mass balance calculations are performed for coolers and heat exchangers, assuming a 0D modeling. Euler fluid dynamics equations are considered for pipes solved in 1D by a finite-volume approach. On the other hand, Colebrook–White and Colburn correlations are implemented for friction and heat transfer calculations.

For the engine cylinder, a 0D modeling is performed, where heat transfer calculations are made using modified and calibrated versions of the Woschni equation. To model turbochargers, characteristic curve data is used to calculate during the simulations, implementing interpolating and extrapolating methods described in Serrano et al. [29], Payri et al. [30] and Galindo et al. [31,32], and friction and heat losses calculations as can be seen in Serrano et al. [33–36]. Finally, the model described in Catalan et al. [37] is used to model the oxygen mass flow through the MIEC membrane implemented in the simulation, which is

calculated at isothermal conditions. Each side (feed and permeate) is also considered a 0D element.

A Wiebe-type function is imposed during the engine calculations to determine the heat released in the cylinder during the combustion process, depending on EGR and spark timing conditions. The parameters of the Wiebe function as duration, shape form and the start of combustion (SOC) are obtained by considering the study made in Serrano et al. [24], which was performed using experimental and CFD methods, as well as 0D-1D thermochemical modeling under oxycombustion conditions with different O_2/EGR proportions. This is widely explained in Appendix B.

3.3. Simplifications

The following simplifications are taken into consideration to simplify the performed calculations for oxycombustion mode operation of the engine:

- A constant effectiveness of 95% is assumed for all the heat exchangers to determine the necessary transfer of thermal energy in each step of air heating. This efficiency value is chosen according to Komminos and Rogdakis [38].
- Outlet air temperature from coolers is set at 25 °C, as well as the ambient conditions.
- Pressure drops of heat exchangers and coolers are negligible.
- Energy consumption of auxiliary elements is considered part of the engine mechanical losses and is included in a general model of the 1.3 l engine friction losses.
- For air, a mass fraction of 77 %N_2/23 %O_2 is used

3.4. Engine control and optimization

For the oxygen production cycle, the global turbocharger efficiency is optimized by changing the position of the stator vanes of the turbines by maximizing Eq. (1):

$$\eta_{\text{total}} = \eta_{\text{LP turbine}} \cdot \eta_{\text{LP compressor}} \cdot \eta_{\text{HP turbine}} \cdot \eta_{\text{HP compressor}} \quad (1)$$

Additionally, the performance of the power cycle is optimized by minimizing brake-specific fuel consumption. This is achieved by changing the spark timing of the combustion, considering a maximum in-cylinder pressure of 15 MPa and maximum temperature of 3000 K as a restriction due to mechanical limitation of the experimental facilities where the combustion laws were obtained.

On the other hand, the O_2/EGR proportion at the engine intake is controlled by changing the position of the stator vanes of the turbine in the exhaust line (element (22) in Fig. 1). As this turbine changes its stator vanes position, the amount of EGR gas driven through the turbine varies, modifying the sweeping gas that goes into the membrane.

Finally, the engine power output for each calculated point of operation is controlled by using a throttle valve (element 2 in Fig. 1) upstream of the low-pressure compressor in the air line. This controls the amount of air that goes into the membrane, which controls the amount of O_2 permeated through the membrane. As an equivalence ratio of 1 is maintained, this strategy helps to ensure the required power output. It must also be mentioned that this valve does not affect the pumping losses of the engine because this throttling is not directly located in the cylinders' intake.

3.5. Turbocharger selection

The geometry and performance maps of the turbomachines considered in this study are obtained from a typical commercial off-the-shelf (COTS) turbocharger implemented in a spark ignition engine. The main details of this turbocharger can be found in Table 4

According to the inlet conditions of the turbomachines, a scale factor is implemented for both turbine and compressor, which allows operating in high-efficiency points for the different engine speeds. For a specific scale factor, non-dimensional groups are remained constant to maintain the similarity in the turbomachines, enabling correct scalability. For turbomachine scaling, non-dimensional mass flow and speed are used, being calculated using Eqs. (2) and (3):

$$\hat{m} = \frac{\dot{m}\sqrt{\gamma RT_{01}}}{D^2 p_{01}\gamma} \quad (2)$$

$$\Omega = \frac{N D}{\sqrt{\gamma RT_{01}}} \quad (3)$$

Then, to calculate efficiencies, adiabatic maps are generated for each turbomachine, being assumed as constant for all the operation points. Consequently, real efficiencies are determined by calculating heat transmission and friction losses that depend on the geometric parameters that are changed due to the applied scale.

The main results are presented in the following section.

Table 4
Specifications of reference turbocharger.

Turbine	
Wheel diameter	37.5 mm
Max. reduced mass flow	12.6 kg s^{-1} K$^{0.5}$ MPa^{-1}
Max. reduced speed	112.2 Hz K$^{-0.5}$
Compressor	
Wheel diameter(mm)	40
Max. corrected mass flow	0.14
Max. corrected speed (krpm)	229
Shaft diameter (mm)	6

Table 5
Operation data of the turbochargers during the engine operation.

	LP Turbo	HP Turbo	O_2/EGR Turbo
Scaling factor	1.8	0.8	0.8
Turbocompressor eff. [%]	45.2–53.6	51.0–53.1	0.1-35.0
Turbine opening [%]	60	60	8.7-49.5
Turbo speed [krpm]	83–166	193–257	2-163

4. Results and discussion

4.1. Turbocharger scaling and performance

Operation data and scaling factors of the different turbochargers that are implemented in the current configuration of the oxycombustion engine are shown in Table 5

First, it should be mentioned how the low-pressure turbocharger has a scale factor almost twice of both high-pressure and O_2/EGR turbochargers. This is due to the lower density handled for both turbine and compressor of this turbocharger, so a higher flow area is required to drive the demanded air for oxygen production. Higher densities allow lower flow areas for the high-pressure turbocharger, thus, a smaller scale value. Finally, to restrict the mass flow through the EGR turbine, reducing the original turbocharger dimensions is necessary to facilitate the control of oxygen and EGR proportion in the intake mass flow. Lower scale values for this turbocharger are not considered because it is not feasible due to the low commercial availability.

Also, it is shown that efficiencies higher than 60% are achieved during the operation of the entire system for the turbomachines that are used to drive the air flow. However, it is important to remark on the significant differences in efficiencies for the O_2/EGR turbocharger, which respond to the small turbine openings required to reach the demanded oxygen concentration at the intake. These small openings lead to a great unbalance between the flow is driven through the turbine and the compressor, which generates low efficiencies in the turbomachines.

Table 6
Engine data at different oxygen mass fractions inlet and cylinder compression ratio - 3000 rpm.

	Power (kW)	BSFC (g/kWh)	IMEP (MPa)	$\dot{Q}_{cyl}$ (kW)	P_{max} (MPa)	T_{max} (°C)	λ
28% O_2							
CR 9.6	88.40	280.32	2.87	21.91	13.56	2252	1.000
CR 12.5	88.40	261.62	2.87	21.41	14.88	2199	1.000
CR 15.0	88.40	253.41	2.87	20.63	14.97	2146	1.000
CR 18.0	88.40	248.36	2.87	20.07	15.06	2102	1.000
30% O_2							
CR 9.6	88.40	280.21	2.87	22.22	13.54	2422	1.000
CR 12.5	88.40	261.46	2.87	21.93	14.94	2378	1.000
CR 15.0	88.40	252.96	2.87	21.24	14.98	2324	1.000
CR 18.0	88.40	247.28	2.87	20.74	15.02	2274	1.000
CR 20.0	88.40	245.10	2.87	20.50	15.03	2245	1.000
32% O_2							
CR 9.6	88.40	283.41	2.85	21.65	12.23	2517	1.000
CR 12.5	88.40	263.62	2.86	21.93	14.24	2499	1.000
CR 15.0	88.40	254.01	2.87	21.87	15.08	2460	1.000
Conv. L0.861	88.40	292.94	2.81	17.16	9.56	2293	0.861
Conv. - L1	75.99	248.03	2.44	16.89	8.56	2390	1.000

4.2. Cylinder compression ratio and oxygen mass fraction effect

This section will study the effect of using different compression ratios and oxygen mass fractions at the intake manifold in a spark-ignition engine operating in oxycombustion, considering the conventional operation as a reference. For this purpose, a comparative analysis of the engine operation at medium speed (3000 rpm) and full load between the oxycombustion and conventional mode is performed. For the conventional mode, two different operation strategies are exhibited in this study: first, decreasing the air-fuel equivalence ratio that allows the reduction of the exhaust temperature. This strategy does not affect the power output but increases fuel consumption and pollution. Second, the stoichiometric combustion ratio is maintained in the cylinders. In the latter strategy, the turbine opening is increased to reduce the air mass flow and pressure at the intake manifold, reducing the exhaust temperature and the power output. These strategies are required to protect the turbocharger turbine. For oxycombustion mode, stoichiometric combustion is performed, assessing oxygen mass fractions between 28%–32%, while the engine compression ratio varies between 9.6–20.

4.2.1. Oxyfuel combustion engine

It is noted in Table 6 that for each intake oxygen mass fraction examined, an increase in the engine compression ratio brings an improvement in fuel consumption, as is expected for a typical Otto cycle. The maximum fuel consumption reduction is exhibited at 30 % O_2, where a decrease of 12.5 % is found when the compression ratio reaches its higher value.

On the other hand, a maximum compression ratio of 20 is reached at 30 % O_2. In contrast, at 32 %, the maximum compression ratio implemented is 15, considering the restriction of 15 MPa in the cylinder. Additionally, for a constant compression ratio, the maximum temperature at the cylinders increases as the oxygen mass fraction rises due to increased in-cylinder reactivity. A maximum temperature higher than 2500 °C is found at 32 % of oxygen mass fraction and a compression ratio of 9.6, being a reasonable value as the in-cylinder temperature restriction is considered.

When these results are compared with the fuel enrichment strategy in conventional combustion, it is seen that fuel consumption is lower for all oxycombustion cases, keeping the same power output. On the other hand, when the stoichiometric air-fuel ratio is kept, a compression ratio higher than 18 is required in oxy-fuel mode to match the BSFC. However, a reduction of 14% in the power output is obtained for this operation in conventional combustion. Also, the values of in-cylinder pressure for the oxycombustion mode are higher, even when the comparison is made for the same engine compression ratio.

In addition, considering the thermodynamic conditions at intake and exhaust manifolds shown in Table 7, an increase in the intake and exhaust pressure is seen as the compression ratio and the oxygen mass fraction are reduced. In addition, the pumping losses (represented in the PMEP) decrease as the compression ratio and the oxygen mass fraction are increased. Moreover, it is naturally expected that higher oxygen mass fractions and lower compression ratios lead to higher temperatures in the exhaust manifold. In this study, the higher temperature is found at 32% and the original compression ratio, with a value of 1170 °C.

The variation of the O_2/EGR turbine opening is also displayed according to the oxygen mass fraction demanded, leading to a greater effective area at the turbine as more oxygen is required.

When compared with conventional cases, oxycombustion scenarios exhibit higher exhaust temperatures. Also, the specific heat capacity ratios of the different O_2/EGR mixings are lower than the air at the conventional intake. Finally, it is shown that the highest intake pressure is found for the conventional case with fuel enrichment, which is reduced by around 0.4 bar when stoichiometric combustion is performed.

These results are explained when the differences in thermochemical properties between CO_2 and N_2 are considered, which affect the behavior of thermodynamic conditions in the cylinders and the combustion parameters. In Table 8, it is shown the main properties of CO_2 and N_2 that affect the combustion performances.

First, CO_2 has a higher molecular weight and density than N_2, which makes CO_2 a heavier molecule, affecting the compressing and pumping work. Furthermore, CO_2 has a higher heat capacity, leading to lower combustion temperatures. On the other hand, CO_2 also has a lower thermal diffusivity, and lower mass diffusivity of oxygen than N_2, reducing the chemical reaction and heat release rates in the early stages of combustion. These changes in the chemical reactions decrease the laminar flame speed when CO_2 is the main bulk gas in the combustion chamber and finally affect the engine performance, as described by Li et al. [40]. The effect of changing N_2 for CO_2 in combustion is shown in studies as those performed by Li et al. [40] and Ditaranto and Hals [41], where they reported a degradation in the combustion process, increasing its duration and reducing the heat release rate peak for the examined conditions due to changes in bulk gas thermochemical properties.

Also, the specific heat capacities ratio is lower in the whole cycle for oxyfuel combustion, as Mohammed et al. also reported [42]. The differences in the specific heat capacities ratio at the intake manifold for this study is seen in Table 7. For Otto-type cycles, this implies a reduction in thermal efficiency.

However, as stated by Serrano et al. [23,24], no knocking issues are expected at high load conditions and advanced spark timings, which

Table 7
Thermodynamic data at the intake and exhaust manifolds at different oxygen mass fractions inlet and cylinder compression ratio — 3000 rpm.

	P_{int} (MPa)	P_{exh} (MPa)	PMEP (MPa)	T_{exh} (°C)	γ_{int}	VGT-O_2/EGR opening (%)
28% O_2						
CR 9.6	0.230	0.247	−0.074	1078	1.312	20.46
CR 12.5	0.216	0.231	−0.067	1034	1.312	20.94
CR 15.0	0.210	0.224	−0.064	1017	1.312	21.20
CR 18.0	0.206	0.220	−0.062	1007	1.312	21.30
CR 9.6	0.213	0.229	−0.071	1118	1.314	25.63
CR 12.5	0.201	0.214	−0.064	1070	1.314	26.09
CR 15.0	0.195	0.208	−0.061	1051	1.314	26.28
CR 18.0	0.191	0.204	−0.058	1038	1.314	26.35
CR 20.0	0.190	0.202	−0.058	1033	1.314	26.34
32% O_2						
CR 9.6	0.202	0.215	−0.069	1170	1.316	30.48
CR 12.5	0.189	0.202	−0.062	1115	1.316	30.54
CR 15.0	0.183	0.195	−0.058	1087	1.316	30.57
Conv.- L0.861	0.252	0.252	−0.042	870	1.400	***
Conv. - L1	0.216	0.247	−0.047	931	1.400	***

Table 8
Comparison of properties between CO_2 and N_2 at 1000 K, 0.1 MPa.
Source: Adapted from [39].

	CO_2	N_2
Molecular weight [g/mol]	44	28
Density [kg/m^3]	0.536	0.341
Heat capacity [kJ/kg K]	1.234	1.167
Thermal diffusivity [m^2/s]	1.1e−4	1.7e−4
Mass diffusivity of oxygen [m^2/s]	9.8e−5	1.3e−4

Table 9
Combustion data at different oxygen mass fractions inlet and cylinder compression ratio - 3000 rpm.

	Duration CA90-CA10 (°)	ST (°ATDC)	SOC (°ATDC)	CA50 (°ATDC)
28% O_2				
CR 9.6	26.42	−37.00	−18.13	1.66
CR 12.5	27.02	−35.00	−16.10	5.40
CR 15.0	27.91	−32.50	−13.98	9.60
CR 18.0	28.46	−30.00	−12.11	12.99
30% O_2				
CR 9.6	21.49	−32.00	−19.94	3.38
CR 12.5	22.01	−30.00	−17.84	5.40
CR 15.0	22.69	−27.10	−15.16	9.70
CR 18.0	23.58	−24.10	−12.80	12.56
CR 20.0	24.49	−22.00	−11.44	14.09
32% O_2				
CR 9.6	18.88	−20.00	−12.74	8.50
CR 12.5	19.05	−20.00	−12.78	8.54
CR 15.0	19.76	−18.00	−11.23	9.80
Conv.- L0.861	16.23	***	6.71	26.50
Conv. - L1	16.44	***	0.00	24.27

allows an improvement in the performance as combustion centering is more feasible at high load conditions than conventional combustion.

Table 9 shows the combustion parameters of conventional and oxy-fuel modes for the studied engine. This table shows the combustion duration, start of combustion (SOC), combustion phasing (CA50) and spark timing (ST), measured in ° of crank angle after the top dead center (ATDC). The duration is computed between the crank angles of 10% and 90% of heat released, and the CA50 is the crank angle at which half the combustion heat has been released. These parameters are computed as a function of several variables, such as the ignition timing and the oxygen/EGR ratio, as explained by Serrano et al. [24]. No information about spark timing was recorded during the experiments for conventional combustion. For oxy-fuel combustion, greater compression ratios lead to less advanced spark timings as the in-cylinder pressure increases, and the maximum pressure restriction must be considered.

Consequently, the start of combustion is delayed, as well as the CA50, while the duration is increased due to a less efficient combustion process. On the other hand, for a constant compression ratio, shorter combustion is seen as the oxygen mass fraction increases due to better reactivity in the cylinder. About combustion phasing, it is well known that optimum values are expected to be between 6° to 10° after the top dead center. In some cases of this study, the CA50 is quite advanced from this range. Nonetheless, the brake-specific fuel consumption shows a plateau around the optimum values found. Thus, moving the spark timing to fit in the mentioned range does not generate significant changes in fuel consumption.

Faster combustion as the oxygen mass fraction increases leads to a rapid increment in pressure and temperature, which restricts the maximum compression ratio that can be implemented. For 32%, the more restricted condition is found, where the higher engine compression ratio is 15. In addition, this also implies that a higher oxygen mass fraction leads to more delayed combustion to avoid combustion issues and fast pressure increases.

When comparing oxyfuel and conventional combustion, conventional combustion has shorter combustion duration, as the air has higher reactivity than O_2/EGR mixing. However, at the used load conditions for comparison, a delay in the start of combustion is required in conventional combustion to avoid knocking issues, affecting the engine efficiency.

A lower load condition is achieved when stoichiometric combustion is implemented for conventional combustion, generating lower pressure and temperature in-cylinder values, thus, reducing knocking problems. The start of combustion can be advanced, improving engine efficiency, even when the power output is affected.

These differences in combustion are seen in Fig. 3, where the heat release law for each evaluated case is exhibited. For oxycombustion cases, a flattening in the heat release laws can be observed as the compression ratio increases due to the delay in the spark advance. Also, higher peaks in the heat release are observed as the oxygen concentration is increases. At 32 % of oxygen mass fraction, it is reached a heat released rate around $0.15\,\mathrm{kJ}\,^{\circ -1}$, which is reduced as the oxygen mass fraction decreases.

Regarding the thermodynamic variables in the cylinders, Fig. 4 shows the pressure–volume diagram for the studied cases. This figure clearly shows the effect of the compression ratio on the maximum pressure for the different cases of oxy-fuel combustion, where the limitation of 15 MPa is observed as a restriction to not advance the spark timing. It is also shown how the delayed start of combustion at conventional combustion leads to lower pressures.

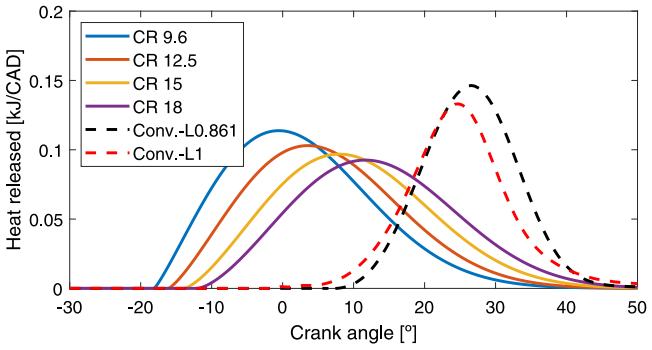

(a) 28 % O_2

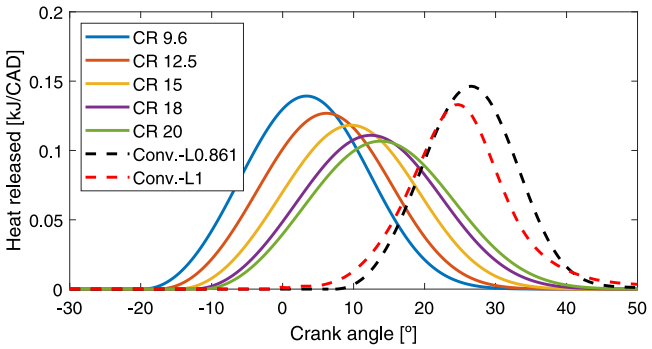

(b) 30 % O_2

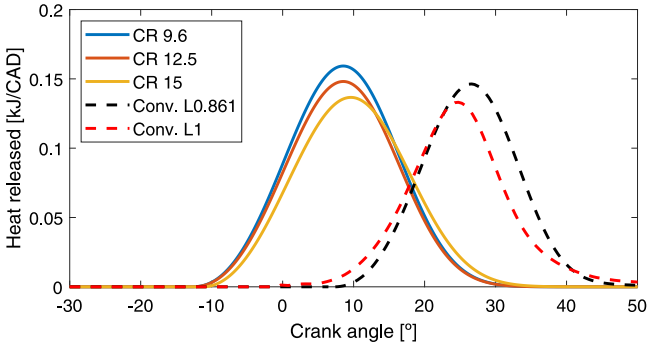

(c) 32 % O_2

Fig. 3. Heat release rate variation for different oxygen mass fractions and compression ratios - 3000 rpm.

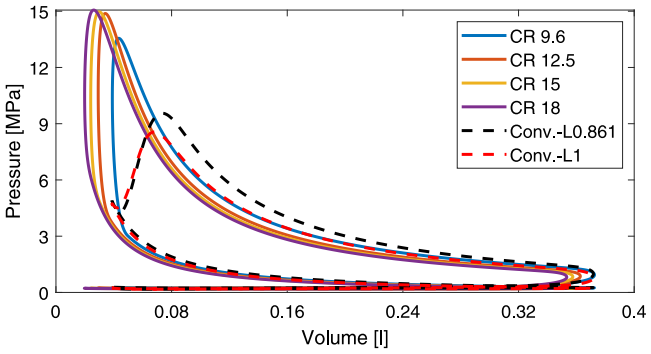

(a) 28 % O_2

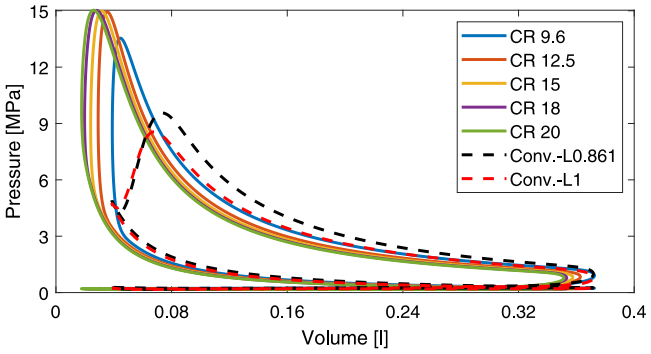

(b) 30 % O_2

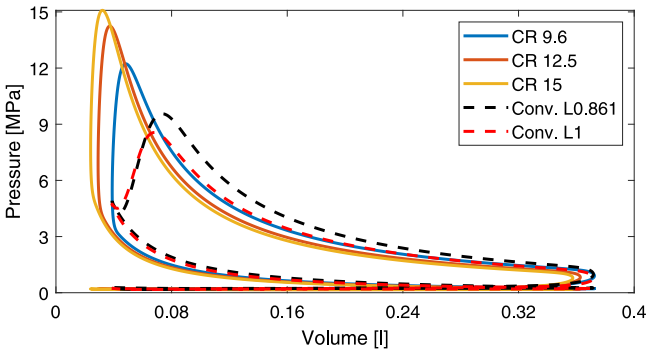

(c) 32 % O_2

Fig. 4. Pressure volume diagram for the studied range of oxygen mass fraction and compression ratio - 3000 rpm.

On the other hand, as a result of both advancing spark timings and increasing the compression ratio, there is a high-pressure area where more power output is obtained. Nonetheless, in the expansion process, the power production is compensated in conventional mode due to a higher specific heat ratio in the cylinder.

Moreover, a magnified version of the pressure–volume diagram focused on the pumping loop is seen in Fig. 5. As stated in Table 8, the heavier molecule of CO_2 increases in the energy required for gas exchange, which is seen in the figure, where the pumping loop area is bigger for oxycombustion cases than conventional ones. Also, as the compression ratio is reduced, the pumping loop is obtained at higher pressures with a greater area, requiring more energy for gas-exchanging processes.

Then, Fig. 6 exhibits the temperature variation with the crank angle for the different studied cases. Higher temperature levels are found in conventional cases due to higher air reactivity, although there is less oxygen in the intake gases than in oxy-fuel combustion. Additionally, a greater slope is seen when the expansion process is performed due to a higher heat-specific ratio of the in-cylinder gases for conventional combustion, which finally reduces the temperature at the exhaust valve opening, resulting in a lower mean exhaust temperature in conventional cases.

Finally, Fig. 7 shows the trapped mass for each cylinder as a function of the crank angle. When the compression ratio increases, the engine performance is improved, for which less fuel is required to produce the same power, and, as a result, less oxygen is demanded. This leads to a lower trapped mass in the cylinders when the oxygen mass fraction remains constant.

On the other hand, for a constant compression ratio, as similar fuel consumption is achieved for the same power, almost the same amount of fuel and oxygen are required for each oxygen mass fraction. For this reason, as the oxygen mass fraction is greater, less trapped mass is demanded at similar oxygen amounts.

Considering the latter, the trapped mass variation is achieved by changing the intake density as the intake pressure is reduced; as for

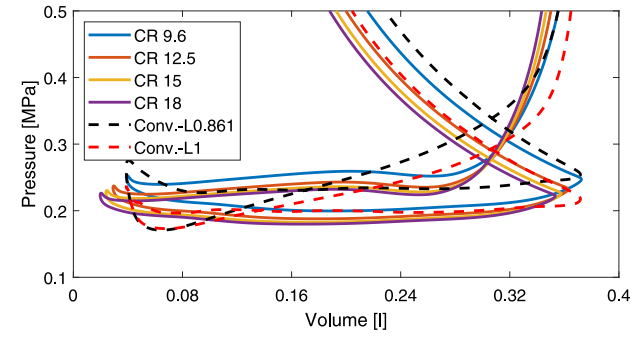

(a) 28 % O_2

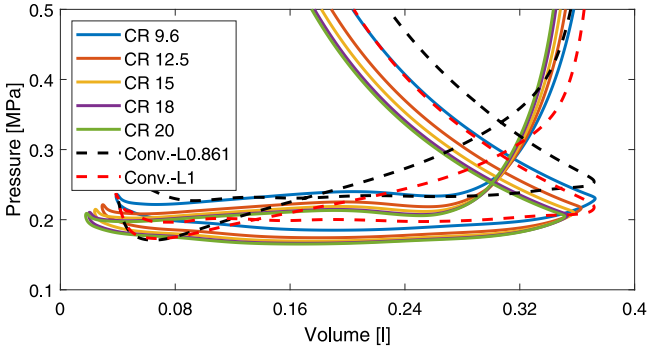

(b) 30 % O_2

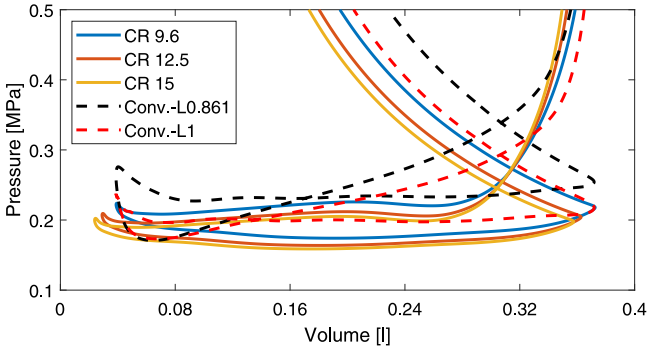

(c) 32 % O_2

Fig. 5. Pumping loop diagram for the studied range of oxygen mass fraction and compression ratio - 3000 rpm.

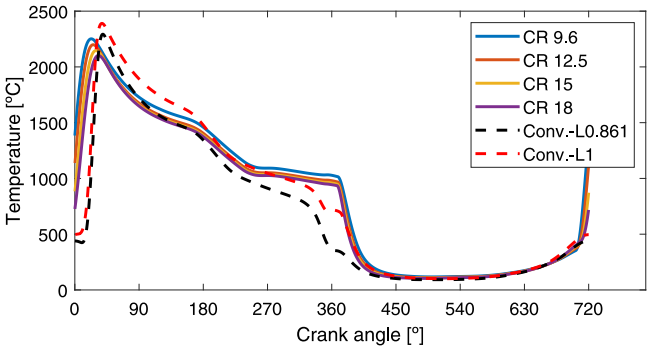

(a) 28 % O_2

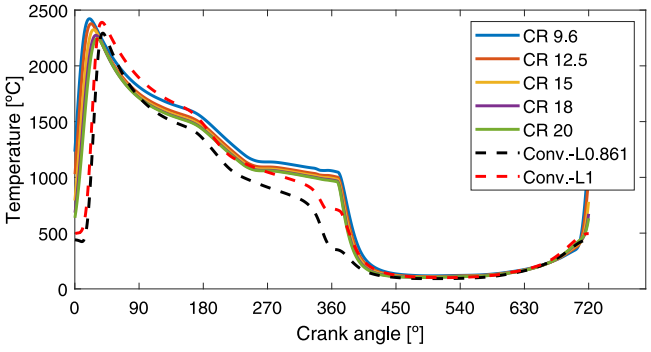

(b) 30 % O_2

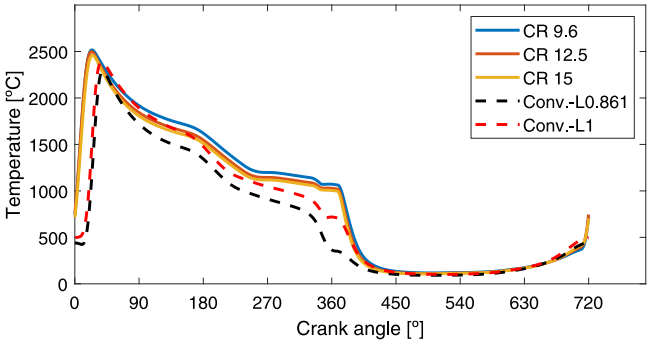

(c) 32 % O_2

Fig. 6. Temperature variation as a function of the crank angle for the studied range of oxygen mass fraction and compression ratio - 3000 rpm.

all the evaluated cases, the engine has the same displacement for each cylinder.

For this, in the conventional cases are found the higher trapped mass, as the oxygen mass fraction in the air is around 23 %, lower than the evaluated oxycombustion cases. Consequently, the highest pressures at the intake and exhaust manifold are found in these scenarios. For the stoichiometric case in conventional mode, as a power reduction is required, there is lower trapped mass and, then, lower manifold pressures.

With this said, it is observed a balance for an oxygen mass fraction of 30 % where there is a trade-off between combustion parameters: Comparing with 28 % of oxygen, there is a delay in the optimum spark advance. However, due to the higher reactivity of the 30 % cases, there is a decrease in the lag between the spark timing and the start of combustion, achieving earlier starts of combustion when comparing constant compression ratios.

On the other hand, compared with 32 % of oxygen, there is a longer combustion duration at 30 % cases. Nonetheless, due to the higher reactivity at 32 %, the spark advance is performed quite later, leading to a delayed start of combustion and affecting the engine performance. This high reactivity in 32 % carries a faster increase in the in-cylinder pressure and temperature as the combustion duration is relatively short. For this reason, higher in-cylinder pressures are reached faster in this case as the compression ratio is incremented, where a limit of 15 is found. Higher compression ratios are restricted, considering the maximum pressure limit in the cylinders and the available range for spark advance at this oxygen mass fraction to avoid combustion issues.

Furthermore, for 28 % of oxygen, as it is the lower oxygen mass fraction in this study, a higher trapped mass is required to obtain the oxygen needed for power production. Consequently, a higher intake pressure is needed, favoring a higher in-cylinder pressure as the compression ratio increases, where a limit of 18 is found in this study. In this sense, there are favorable conditions at 30 % for the combustion and manifold conditions, allowing a compression ratio of 20, achieving the best performance for the studied cases.

Finally, when both combustion modes are compared, it is seen that the primary sources of the consumption differences are the fuel

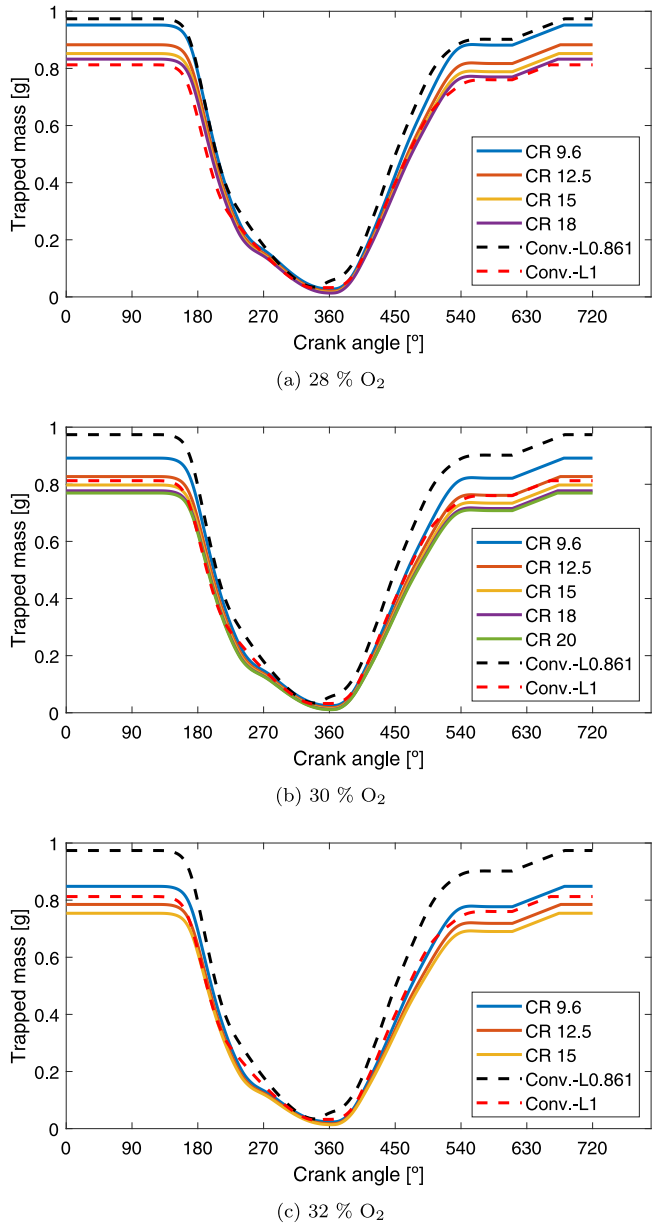

(a) 28 % O_2

(b) 30 % O_2

(c) 32 % O_2

Fig. 7. Cylinder trapped mass variation as a function of the crank angle for the studied range of oxygen mass fraction and compression ratio - 3000 rpm.

enrichment in the conventional mode and the start of combustion delaying to ensure stability, which can even be after the top dead center at the expansion stroke. However, when stoichiometric combustion is performed, the power decrease required to reduce the exhaust temperature also allows an advance in the start of combustion, favoring the fuel consumption in the engine.

4.2.2. Oxygen production cycle

This section explains the performance of the oxygen production cycle coupled to the engine operation as the oxygen requirements and available energy vary according to the operation point.

In Table 10 is seen the variation of the air conditions at the membrane inlet for the different oxy-fuel cases. As the compression ratio increases, the exhaust manifold temperature lowers, and the recoverable energy to heat the air decreases. This explains the reduced heat exchange to the air line and a lower temperature at the membrane feed side inlet.

Table 10
Air conditions at membrane inlet at different oxygen mass fractions inlet and cylinder compression ratio - 3000 rpm.

	$\dot{m}_{air}$ (kg/h)	P_{feed} (MPa)	T_{feed} (°C)	$\dot{Q}_{HE}$ (kW)
28% O_2				
CR 9.6	446.7	0.420	1037	141.2
CR 12.5	421.7	0.392	992	126.9
CR 15.0	410.5	0.381	975	121.2
CR 18.0	403.7	0.374	965	117.8
30% O_2				
CR 9.6	443.9	0.420	1067	145.2
CR 12.5	419.0	0.392	1019	130.2
CR 15.0	407.5	0.380	1000	124.0
CR 18.0	399.9	0.372	987	119.9
CR 20.0	397.1	0.369	982	118.5
32% O_2				
CR 9.6	445.6	0.426	1111	152.3
CR 12.5	419.7	0.396	1056	135.4
CR 15.0	407.4	0.382	1028	127.5

Table 11
Membrane operation at different oxygen mass fractions inlet and cylinder compression ratio - 3000 rpm.

	$p_{feed,O_2}/p_{perm,O_2}$ (-)	T_{memb} (°C)	$\dot{m}_{O_2}$ (g/s)	η_{memb} (%)
28% O_2				
CR 9.6	1.142	1020	22.97	81.77
CR 12.5	1.158	975	21.44	81.03
CR 15.0	1.168	958	20.75	80.64
CR 18.0	1.172	948	20.35	80.42
30% O_2				
CR 9.6	1.121	1043	22.95	82.63
CR 12.5	1.140	996	21.42	81.68
CR 15.0	1.149	976	20.71	81.25
CR 18.0	1.155	963	20.26	80.96
CR 20.0	1.157	959	20.08	80.83
32% O_2				
CR 9.6	1.106	1077	23.22	82.98
CR 12.5	1.125	1023	21.60	81.98
CR 15.0	1.136	996	20.82	81.41

At the same time, this reduction in the available energy reduces the air mass flow and the inlet pressure of air at the membrane, as there is less energy to drive the turbines that move the air compressors.

However, as was seen in the previous section, the compression ratio increase improves the fuel consumption in the engine. Considering the same power output for each studied case, the reduction in fuel consumption implies less oxygen production at the membrane for the combustion in the cylinders. This is seen in Table 11, where there is a reduction in oxygen production at the membrane as the compression ratio increases.

On the other hand, it is also seen an increase in the mean oxygen partial pressure ratio, the driving force of the oxygen diffusion through the membrane. As the temperature is reduced, the oxygen permeation is less favorable. The oxygen partial pressure at the feed side outlet increases as less oxygen is permeated, leading to a higher mean oxygen partial pressure at the feed side. Additionally, on the permeate side, related to the intake and exhaust manifold conditions, the pressure is also lower, reducing the oxygen partial pressure at the permeate side.

These effects are clarified in Fig. 8, where the operation points of the different studied cases are depicted over a membrane map with different isolines of production.It is seen how higher compression ratios lead the membrane to work at lower temperatures and higher oxygen pressure ratios while oxygen production is reduced. Additionally, it could be remarked that the effect of the oxygen mass fraction, whose increase generates higher temperatures in the exhaust manifold

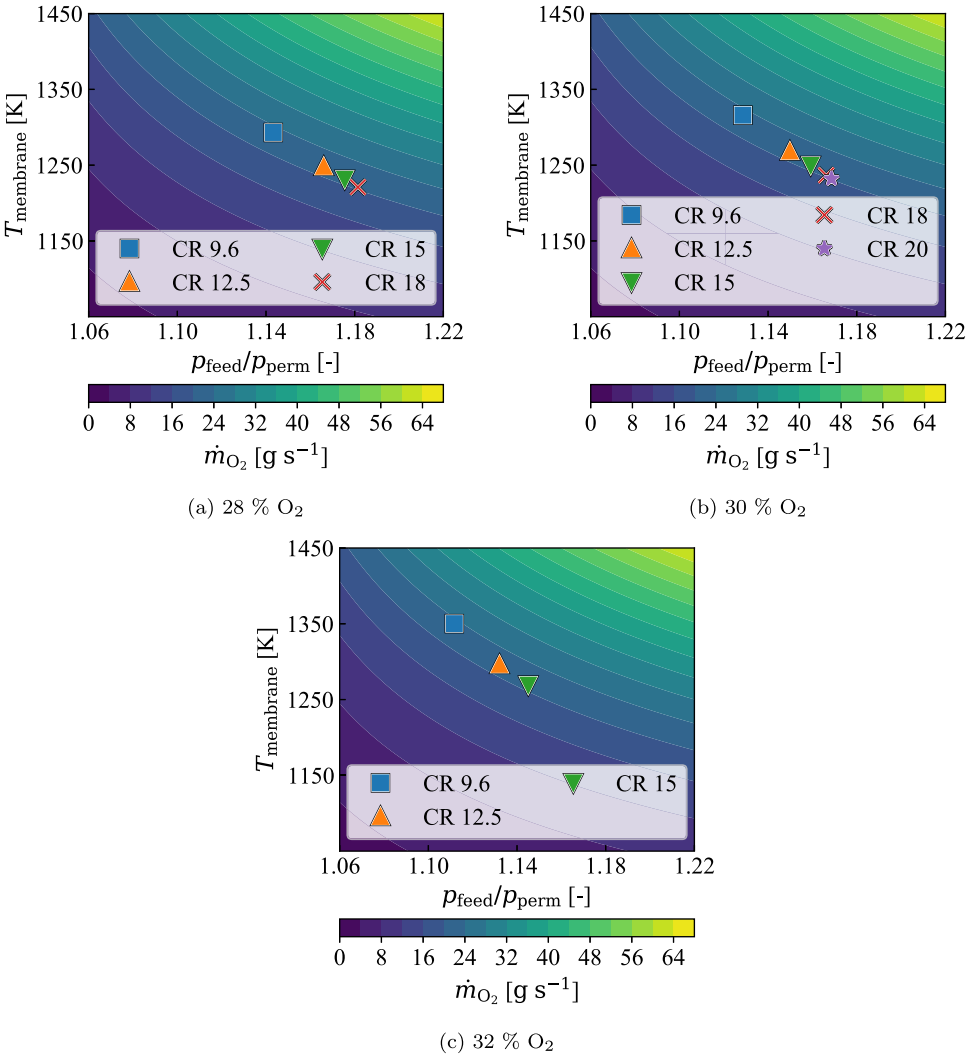

(a) 28 % O_2

(b) 30 % O_2

(c) 32 % O_2

Fig. 8. Membrane map operation at different oxygen mass fractions inlet and cylinder compression ratio - 3000 rpm.

and, consequently, in the air mass flow at the feed side inlet of the membrane, improves oxygen production.

Considering this, it is also defined the membrane efficiency as the ratio of the permeated oxygen through the membrane with the oxygen mass flow brought through the air to the feed side inlet. Operating at higher compression ratios decreases the membrane efficiency, as it operates at lower temperatures.

In other words, there is a precise coupling between the operation of both power and oxygen production cycles. As the engine efficiency is improved, the available energy to drive the oxygen production cycle is reduced, considering a decrease in the exhaust temperature. Therefore, the air heating is affected, and the air temperature at the feed side inlet of the membrane is reduced.

Then, there is a reduction in the available energy at the expansion stages (elements 12 and 14 of Fig. 1), decreasing the mass flow and pressure at the feed side inlet of air, creating a feedback effect where the pressure and mass flow reduction implies less enthalpy flow for the turbines until an energy balance in the turbomachines is achieved.

At the same time, a more efficient engine requires a lower fuel consumption for power production by definition, which implies a lower oxygen production requirement. Thus, both phenomena in the system operation are complementary, obtaining an autonomous system whose available energy for oxygen production matches its needs and achieving a higher global system efficiency as the compression ratio increases.

4.3. Full load performance

A full load study is extended at low and high engine speeds, comparing the 1500 to 5000 rpm range. For oxyfuel combustion cases, this section considers the full load calculations operating at 30% of oxygen mass fraction at the intake, which exhibits the best performance as was explained, working at a compression ratio of 9.6, which is the original engine value that works as a reference, and 20, which exhibited the best performance at medium engine speed (3000 rpm). This is performed to assess the viability of applying the most feasible conditions found in the medium-speed study at different engine speed conditions. The fuel consumption of the different speeds is compared, whose differences are explained in terms of combustion parameters and thermodynamic behavior of the in-cylinder gases. Also, the oxygen production cycle operation is analyzed in these cases to determine ranges in membrane operation conditions for the studied speed range..

4.3.1. Conventional and oxycombustion comparison

Fig. 9 shows the engine's power and brake-specific fuel consumption of the engine working at conventional and oxycombustion modes. For the conventional case, experimental and simulated data are shown, while for oxycombustion mode, the results are obtained by simulating the mentioned conditions.

For power comparison, it is seen how both oxyfuel combustion cases match the full load power output obtained in the conventional

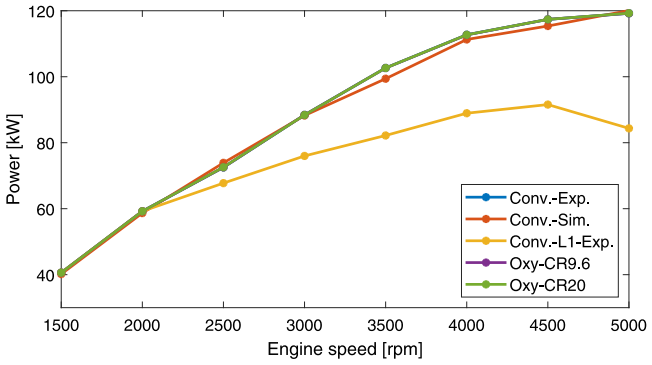

(a) Power (kW)

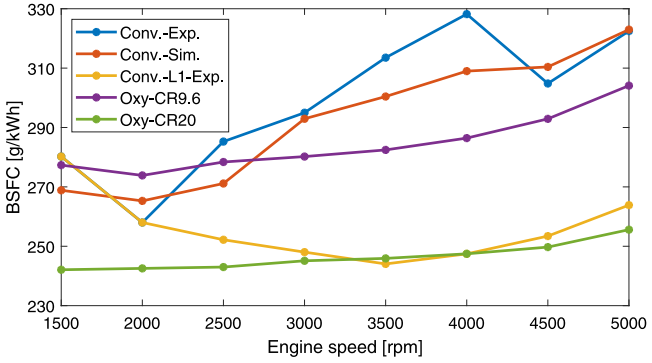

(b) BSFC (g/kWh)

Fig. 9. Comparison of full load engine performance at different speeds.

operation, where lines in the figure are overlapped due to this matching. When conventional combustion operation is restricted to stoichiometric, the power at speeds higher than 2000 rpm is reduced considerably.

On the other hand, for fuel consumption, it is seen that for conventional operation, both simulated and experimental data exhibit the same consumption trends, where at higher speeds the fuel requirement increases as more fuel enrichment is needed to reduce the exhaust temperature. However, as stoichiometric combustion is used, fuel consumption decreases, obtaining the typical trend of an internal combustion engine working under stoichiometric conditions.

For oxycombustion cases, two identical curves whose displacement results from the compression ratio increment are obtained. When the original compression ratio is used in oxyfuel combustion, the fuel consumption is comparable to the conventional operation when fuel enrichment is performed, being better at high speeds. Also, when the compression ratio is varied to 20, the fuel consumption can be compared with the conventional performance using stoichiometric combustion, where the fuel consumption at low and high speeds is better for the oxycombustion case.

Table 12 shows the primary engine data for low (1500 rpm) and high (5000 rpm) speeds. In conventional mode, fuel enrichment is not required to maintain the exhaust temperature for 1500 rpm as seen for 5000 rpm. At low speed, when the compression ratio is kept at 9.6, fuel consumption is 3.2% higher in the oxyfuel combustion case than in the conventional one. A considerable difference in the in-cylinder maximum pressure and similar maximum temperatures are also seen. When a compression ratio of 20 is considered, a reduction of 10% in fuel consumption is seen, where the maximum in-cylinder pressure is near the imposed pressure restriction, and there is a reduction of approximately 200 °C in the maximum in-cylinder temperature.

At high speed, using the original compression ratio, there is a reduction of 5.9% in fuel consumption for the oxy-fuel combustion case compared with the conventional case with fuel enrichment. Further, there is an increment of 15.2% considering stoichiometric combustion. Also, the pressure in oxy-fuel combustion is considerably higher, while the maximum temperature is reduced in oxycombustion, as observed for low speed. In addition, when the compression ratio is increased to 20, a remarkable reduction in fuel consumption is obtained, with a decrease of 21.1% compared with the fuel enrichment scenario at conventional combustion and 3.4% when stoichiometric combustion is considered. On the other hand, there is a reduction of 30% in the power output when stoichiometric combustion is implemented at this speed.

Further, variations in thermodynamic conditions at the intake and exhaust manifolds are shown in Table 13. Higher pressures are seen at both intake and exhaust manifolds in the conventional case for both low and high speeds. Also, as liquid water is avoided at the intake manifold to protect the mechanical integrity of the cylinders, there are higher temperatures (85 °C) in oxy-fuel combustion mode. When exhaust temperatures are compared, higher values are obtained at oxy-fuel combustion (>1000 °C).

These differences can be explained by considering the combustion parameters differences, as was performed in the medium-speed study. In Table 14 it is seen the differences in combustion parameters for low and high speeds are seen. For both engine speeds, it is seen that combustion duration is shorter for conventional mode (around 50%) when compared with oxy-fuel combustion. Nonetheless, combustion delay is required in conventional cases to avoid combustion issues, as has been explained.

At low speeds, an approximately 30° delay is observed between the start of combustion of conventional and oxy-fuel combustion, affecting the combustion centering, thus, the engine performance. For high speed, it is seen that the power reduction for using stoichiometric combustion also allows more advanced combustion, which improves the engine performance. However, a clear difference in the combustion start still generates a gap in both combustion modes performance at high speed. The differences in combustion parameters are better observed in Fig. 10, where combustion differences are explicitly seen.

The differences in in-cylinder thermodynamic variables product of these combustion variances are also explained. Fig. 11 shows the pressure–volume and temperature–volume diagrams for low and high speeds. At low speed, the difference in the start of combustion between conventional and oxy-fuel combustion modes is remarked in both diagrams, allowing higher pressures in oxy-fuel.

This effect is not strong at high speed, where more advanced combustion starts are allowed in conventional combustion, achieving similar pressure levels compared with oxy-fuel. On the other hand, for conventional cases, a greater area in the diagram at the expansion stroke is still observed, similar to medium speed, resulting from a higher heat-specific ratio, as has been explained. On the other hand, the T-V diagram exhibits the in-cylinder temperature behavior at low and high speeds. As a result of a higher heat-specific ratio, greater slopes are seen in the temperature evolution for the conventional mode, allowing lower temperatures at the exhaust manifold when valves are opened.

Additionally, the pumping loop of the pressure–volume diagram for low and high speeds is presented in Fig. 12. A positive pumping loop is obtained at the conventional low-speed operation mode. In contrast, a reduced loop area is expected for the slight difference between manifold pressures in oxycombustion. This explains part of the fuel consumption divergence at the original compression ratio. Otherwise, this pumping loop benefit is diluted at high speed, as a negative loop is presented for both combustion modes with similar working areas. This behavior in the pumping loop explains the differences in the PMEP shown in Table 13. For the trapped mass diagram, higher trapped masses are achieved for the conventional mode due to a lower oxygen concentration in the air, leading to higher intake pressures, as explained.

Table 12
Engine data at low and high speeds - Full load.

	Power (kW)	BSFC (g/kWh)	IMEP (MPa)	P_{max} (MPa)	T_{max} (°C)	λ
1500 rpm						
Conv. - L1	40.18	268.86	2.51	7.19	2333	1.000
Oxycomb. CR9.6%–30% O_2	40.61	277.57	2.56	11.67	2348	1.000
Oxycomb. CR20%–30% O_2	40.61	242.13	2.59	14.79	2147	1.000
5000 rpm						
Conv.- L0.812	120.07	322.97	2.30	9.86	2265	0.812
Conv. L1	84.35	263.86	1.76	8.57	2447	1.000
Oxycomb. CR9.6%–30% O_2	119.28	304.06	2.53	12.16	2326	1.000
Oxycomb. CR20%–30% O_2	119.21	254.79	2.51	14.93	2274	1.000

Table 13
Intake and exhaust manifolds data at low and high speeds - Full load.

	P_{int} (MPa)	T_{int} (°C)	P_{exh} (MPa)	T_{exh} (°C)	PMEP (MPa)
1500 rpm					
Conv. - L1	0.247	38.28	0.211	877.6	0.053
Oxycomb. CR9.6%–30% O_2	0.200	84.85	0.194	1054.9	−0.007
Oxycomb. CR20%–30% O_2	0.178	84.85	0.174	946.3	−0.007
5000 rpm					
Conv.- L0.812	0.238	43.36	0.327	867.4	−0.257
Conv. - L1	0.164	34.74	0.231	942.8	−0.163
Oxycomb. CR9.6%–30% O_2	0.191	84.85	0.197	1160.16	−0.215
Oxycomb. CR20%–30% O_2	0.163	84.85	0.175	1047.45	−0.167

Table 14
Combustion data at low and high speeds - Full load.

	Duration (°)	SOC (°)	CA50 (°)
1500 rpm			
Conv. - L1	15.37	15.61	34.23
Oxycomb. RC9.6%–30% O_2	21.64	−18.85	4.91
Oxycomb. RC20%–30% O_2	23.28	−13.45	11.81
5000 rpm			
Conv. - L0.812	16.80	0.28	20.64
Conv. - L1	15.99	−9.50	12.53
Oxycomb. RC9.6%–30% O_2	20.95	−21.09	1.90
Oxycomb. RC20%–30% O_2	22.67	−14.92	10.14

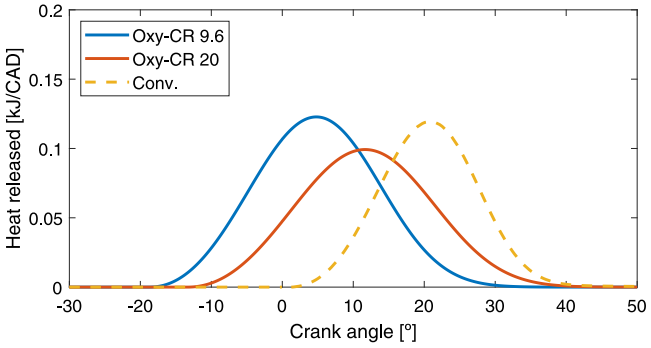

(a) Low speed (1500 rpm)

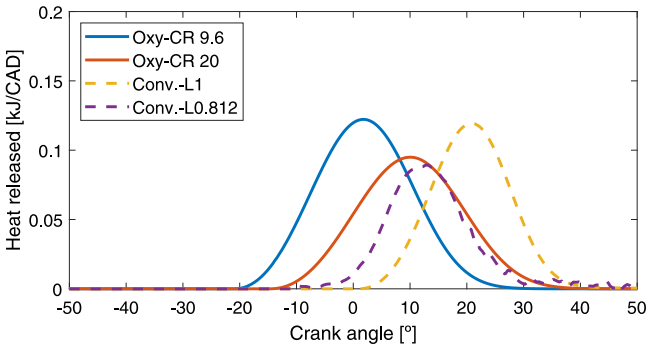

(b) High speed (5000 rpm)

Fig. 10. Heat release law at low and high speed.

That said, for low speeds, it is seen that the primary sources of fuel consumption differences are in combustion, which is longer for oxy-fuel combustion but can be advanced around 30°, compared with conventional, due to its characteristics. Moreover, in conventional mode, a positive pumping loop is observed, improving the gas exchange and compensating for the required combustion delay.

The primary sources of fuel consumption differences for high speeds are the required enrichment to reduce exhaust temperature, which remarkably harms performance. When stoichiometric combustion is performed, a notable reduction in fuel consumption is achieved, reducing the power output. In addition, the combustion characteristics play an important role, as explained for low and medium speeds.

Finally, it is worth mentioning that, due to oxyfuel characteristics, an increase in the compression ratio can be performed, achieving promising fuel consumption. Therefore, full load power output is achieved in this scenario, obtaining comparable fuel consumption as when stoichiometric combustion is performed in conventional mode, accomplishing both benefits of conventional combustion scenarios.

4.3.2. Oxygen production cycle performance

In Fig. 13 is shown the performance of the membrane for the original compression ratio and increased to 20, using 30% of oxygen in oxy-fuel combustion. As was explained, an increment in the compression ratio reduces in the exhaust temperature, reducing the available energy to produce oxygen. This is compensated due to a decrease in fuel consumption, reducing the oxygen needed.

For the original compression ratio, the operating temperature of the membrane is ranged between 918 °C to 1124 °C, while for 20, the temperature is reduced from 800 °C to 1009 °C, achieving an average temperature reduction of 100 °C in the whole speed range when the compression ratio is increased.

At the same time, the reduction of membrane temperature increases in the oxygen partial pressure, which can be observed in Fig. 13.

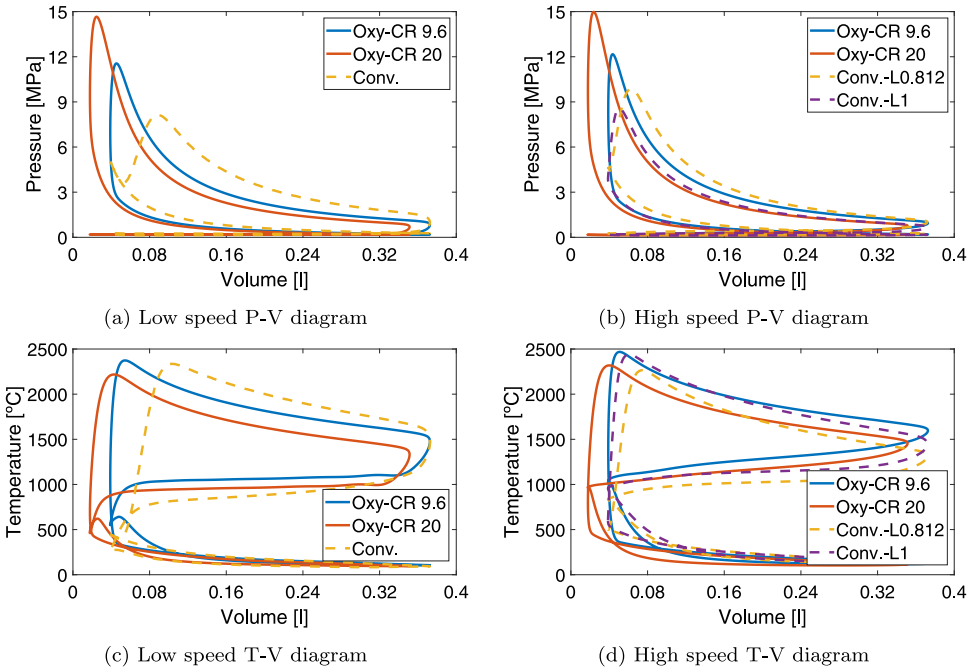

(a) Low speed P-V diagram (b) High speed P-V diagram

(c) Low speed T-V diagram (d) High speed T-V diagram

Fig. 11. Pressure–volume and temperature–volume diagrams at low and high speed.

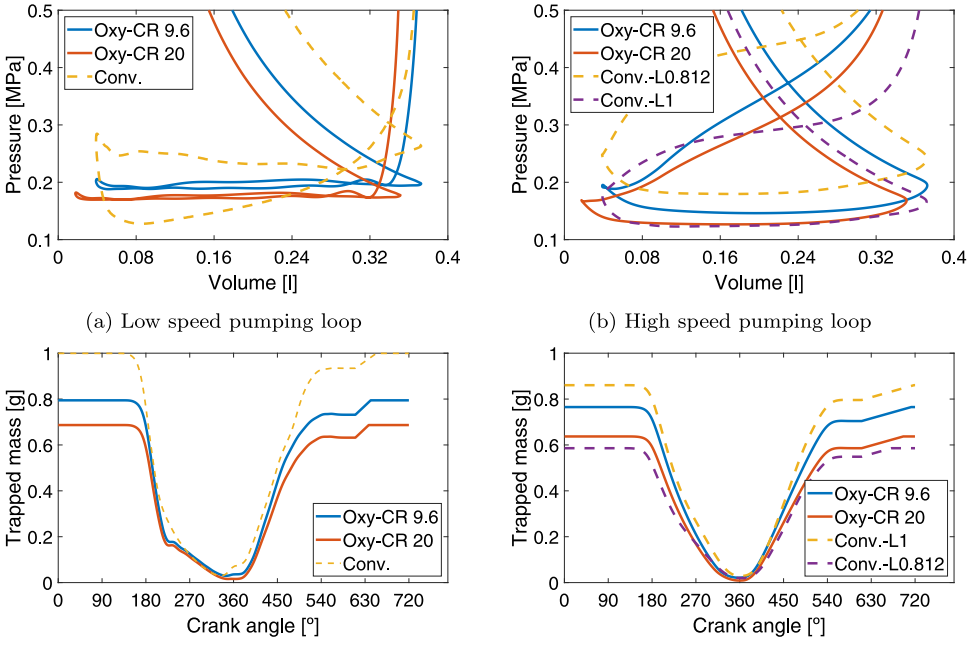

(a) Low speed pumping loop (b) High speed pumping loop

(c) Low speed trapped mass (d) High speed trapped mass

Fig. 12. Pumping loop and trapped mass at low and high speed.

Thereupon, the turbomachinery performance in all the engine speed ranges is also worth mentioning. For the selected turbomachinery in the oxygen production cycle, it is seen that the operation is performed in a comfortable zone for both air-driving compressors, being distant from the choke and surge line and achieving high efficiencies. As mentioned, there is a lower air mass flow and compression ratio at high engine compression ratios. This explains the differences when operating the turbomachines in the oxy-fuel engine for both studied scenarios. On the other hand, the O_2/EGR compressor does not offer a remarkable boost in the intake pressure of the engine for both studied compression ratios. This results from a noticeable unbalance between the mass flow that goes through the EGR turbine associated with this compressor (element 22 in Fig. 1) and the stream driven by the compressor itself, which leads to a low efficiency for the whole turbomachine.

The turbomachines performance maps for both engine compression ratios scenarios can be seen in Appendix A.

4.3.3. *Engine limitations*

The authors have identified operation limits regarding the integrity of components and energy availability for oxygen production. The latter section shows that membrane operation is performed at temperatures higher than 1000 °C for high engine speeds using the original compression ratio. These temperatures can risk the integrity of the membrane,

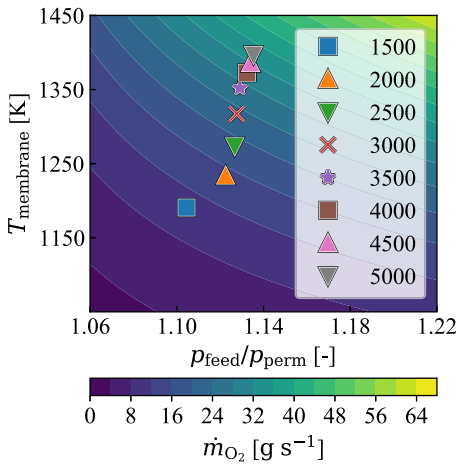

(a) CR 9.6

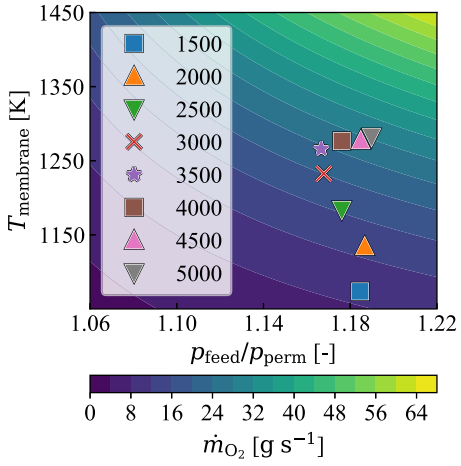

(b) CR 20

Fig. 13. Membrane operation at engine full load.

affecting the crystalline structure of the MIEC material and its support. Additionally, as the outlet streams of the membrane go out at a similar temperature to the operative one, there is a risk of damaging the turbomachines. On the other hand, increasing the compression ratio reduces the energy in the exhaust line, which decreases the operating temperature of the membrane and the turbomachines, leading to a safer operation for these components.

Moreover, for lower engine speeds than 1500 rpm, there is a considerable reduction in the available energy for oxygen production, which is seen in this study as lower engine speeds are not presented. There is not only a reduction of temperature but also a decrease in the feed pressure and the air mass flow in the oxygen production cycle, affecting the whole system operation.

The compression ratio can be crucial for the part-load operation to determine operative limits. As mentioned, the engine compression ratio increase can benefit turbomachines and membrane integrity. However, this affects the lower load that can be achieved, as the available energy is reduced. Further research must be performed to find energy availability limitations at part-load using different compression ratios. Nonetheless, a study performed by Serrano et al. [43] shows that a system similar to that of the present paper that uses a compression-ignition engine can be operated until 50% of the maximum load for each examined engine speed. The reduction of the load is explained due to the reduction of available energy in the exhaust gases for oxygen production. Comparable results are expected in the system presented in this study.

Finally, it is also seen that increasing the oxygen concentration at the intake has a remarkable rise in the exhaust manifold temperature, the operating temperature of the membrane, and the turbomachines. For the highest oxygen concentration that is studied (32%), it was found that the room to increment the compression ratio is the most limited, leading to keeping high temperatures of operation in the mentioned components (higher than 1000 °C). On the other hand, the lowest oxygen concentration (28%) could lead to reduced energy availability to operate at low speeds and loads. Thus, an oxygen concentration of 30% can balance both effects, where reasonable protection of components is obtained, as well as energy availability to operate in a wide range of loads and speeds.

5. Conclusions

An oxycombustion spark-ignition engine coupled to an oxygen production cycle based on a MIEC-type membrane is studied in this paper. The effect of varying the compression ratio and the oxygen mass fraction is first studied in both engine and oxygen production cycles for medium engine speed (3000 rpm), comparing its performance with the conventional engine operation.

As expected, increasing the compression ratio in oxycombustion is beneficial for fuel consumption, as expected. However, delaying the start of combustion is necessary to keep the maximum pressure limit, reducing the potential engine performance. Additionally, greater oxygen concentrations enhance the reactivity in the cylinder, reducing the combustion duration. However, it also demands a delay in the start of combustion to avoid combustion issues, affecting fuel consumption.

An optimum case at 30% of oxygen mass fraction was found, where trade-off conditions were identified, allowing the increase of engine compression ratio to 20 and achieving the best engine performance in this study.

The main difference between oxycombustion and conventional operation is in bulk gas: CO_2 for oxycombustion and N_2 for conventional cases. Their physicochemical properties lead to differences in combustion and thermodynamical behavior, demanding more delayed combustion to avoid instabilities for the conventional scenario and worse performance in the expansion stroke due to a higher heat-specific ratio for oxycombustion.

For the oxygen production cycle performance, it is seen that increasing the compression ratio implies a reduction in the available energy for oxygen production but also lower fuel consumption and, consequently, less oxygen required. Therefore, an autonomous coupled system was obtained, allowing changes in the working conditions and generating the demanded oxygen according to the power output needed.

In addition, the study is extended by considering the oxycombustion engine working at 30% of intake oxygen mass fraction using the original compression ratio (9.6) and 20 at a wide range of engine speeds (1500–5000 rpm), being compared with the conventional operation.

The oxycombustion engine can achieve the full load power values taken as a reference in both scenarios, showing a sustainable system from an energy view in the studied speed range. Using the original compression ratio, the fuel consumption of the oxycombustion engine has similar values to the conventional case implementing fuel enrichment, while using a compression ratio of 20 has similar fuel consumption to the conventional case operating with stoichiometric combustion.

That said, the oxy-fuel combustion used in a spark-ignition engine coupled exhibits a promising performance, where reference load conditions of the conventional mode can be achieved. In addition, high compression ratios and advanced spark timings can be operated, leading to significant benefits in fuel consumption.

Also, an oxygen production cycle based on a MIEC membrane can be used in the engine operation to fulfill the oxygen requirements by taking advantage of the exhaust gases energy. This cycle has demonstrated to be capable of operating in different oxygen mass fractions and compression ratios, as well as engine speeds and load conditions.

Particular attention must be given to the operative limits found in the study. For high oxygen concentrations and low compression ratios, good performances have been found regarding fuel consumption. However, high temperatures (above 1000 °C) are observed in the membrane and turbomachines in these cases, which can risk the integrity of these components. On the other hand, limits regarding energy availability are expected at part-load operation and low speeds, significantly as the compression ratio increases. A balance for components integrity and energy availability is expected to be around an oxygen concentration of 30% at the engine intake.

Further research could be performed regarding the experimental refinement of the implemented combustion laws for the different compression ratios used in this study to find more realistic limits regarding combustion parameters and load. On the other hand, modifications in the heat exchange network can be performed, which allows the reduction of inlet temperature at critical elements such as turbomachines and as the proper exploitation of the exhaust gases energy to drive the oxygen production in a wide range of operation.

In addition, the authors expect to perform studies regarding the partial load behavior of this engine, searching for operative boundaries, especially in terms of energy availability. Finally, as the oxycombustion calculations were performed in stoichiometric conditions to obtain exhaust gases composed of carbon dioxide and water vapour to facilitate the carbon capture from the exhaust gases, the coupling of a carbon capture system is expected to be performed, considering its thermodynamic implications.

Nomenclature

ATDC	After top dead center
$BSFC$	Brake specific fuel consumption
CA-10	Crank angle where 10% of the fuel heat has been released
CA-50	Combustion phasing
CA-90	Crank angle where 90% of the fuel heat has been released
CAS	Cryogenic air separation
CI	Compression-ignition engine
COTS	Commercial off-the-shelf
CR	Engine compression ratio
EGR	Exhaust gas recirculation
η	Efficiency
η_{memb}	Membrane efficiency
γ	Specific heat ratio
HCCI	Homogeneous Charge Compression Ignition
HC	Hydrocarbons
HE	Heat exchanger
HP	High pressure
ICE	Internal combustion engine
$IMEP$	Indicated mean effective pressure
λ	Oxidizer-fuel equivalence ratio
LP	Low pressure
MIEC	Mixed ionic and electronic conducting
$\hat{m}$	Turbomachines nondimensional mass flow
$\dot{m}_{air}$	Air mass flow
$\dot{m}_{HPT}$	Air mass flow through heat exchange network bypass
$\dot{m}_{HPT}$	Air mass flow between elements 5 and 12 bypass
$\dot{m}_{O_2}$	O_2 mass flow permeated through the membrane
$\dot{m}^*$	Compressor corrected mass flow
N^*	Compressor corrected speed
ω	Turbomachines nondimensional speed
π_{comp}	Compressor total-to-total pressure ratio
P_{feed}	Pressure of the membrane feed flow
P_{exh}	Pressure of exhaust manifold
P_{int}	Pressure of intake manifold
P_{max}	Maximum in-cylinder pressure
PMEP	Pumping Mean Effective Pressure
PM	Particulate matter
p_{feed,O_2}	Average O_2 partial pressure of the membrane feed flow
p_{perm,O_2}	Average O_2 partial pressure of the membrane permeate flow
$\dot{Q}_{cyl}$	Heat released from cylinders to environment
$\dot{Q}_{HE}$	Total heat exchanged by the air mass flow
$\dot{Q}_{HE-9}$	Heat exchanged in element 9
$\dot{Q}_{HE-10}$	Heat exchanged in element 10
SOC	Start of combustion
T_{exh}	Temperature of exhaust manifold
T_{feed}	Temperature of the membrane feed flow
T_{int}	Temperature of intake manifold
T_{max}	Maximum in-cylinder temperature
$\dot{W}$	Power

CRediT authorship contribution statement

José Ramón Serrano: Conceptualization, Validation, Resources, Writing – review & editing, Supervision, Project administration, Funding acquisition. **Francisco José Arnau:** Conceptualization, Methodology, Software, Writing – review & editing, Funding acquisition. **Luis Miguel García-Cuevas:** Conceptualization, Methodology, Software, Writing – review & editing, Visualization, Supervision. **Fabio Alberto Gutiérrez:** Methodology, Validation, Formal analysis, Investigation, Data curation, Writing – original Draft, Writing – review & editing, Visualization, Funding acquisition.

Declaration of competing interest

The authors declare the following financial interests/personal relationships which may be considered as potential competing interests:

Fabio Alberto Gutiérrez reports financial support was provided by Conselleria de Innovación, Universidades, Ciencia y Sociedad Digital de la Generalitat Valenciana. José Ramón Serrano reports financial support was provided by Conselleria de Innovación, Universidades, Ciencia y Sociedad Digital de la Generalitat Valenciana. Francisco José Arnau reports financial support was provided by Spain Ministry of Science and Innovation. Francisco José Arnau, José Ramón Serrano and Luis Miguel García-Cuevas has patent ##ES2751129B2 issued to Consejo Superior de Investigaciones Científicas CSIC y Universitat Politècnica de València.

Data availability

Data will be made available on request

Acknowledgments

The authors want to acknowledge the institution “Conselleria de Innovación, Universidades, Ciencia y Sociedad Digital de la Generalitat Valenciana” and its grant program “Subvenciones para la contratación de personal investigador de carácter predoctoral” for doctoral studies (ACIF/2020/246) funded by The European Union. This work has been partially supported by Grant PID2021-123351OB-I00 funded by MCIN/AEI/10.13039/501100011033 and, as appropriate, by “ERDF A way of making Europe”. In addition, this research has been also supported by Grant CIPROM/2021/061 funded by Generalitat Valenciana. Funding for open access charge: CRUE-Universitat Politècnica de València.

Appendix A. Compressors performance maps

See Figs. A.14 and A.15.

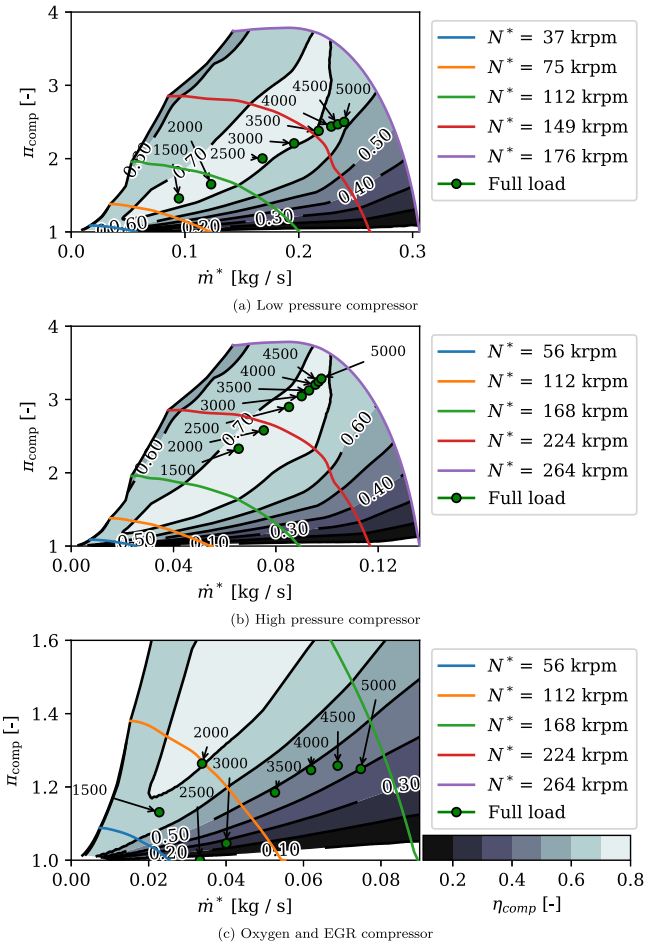

Fig. A.14. Compressor maps of the oxygen production cycle - CR9.6.

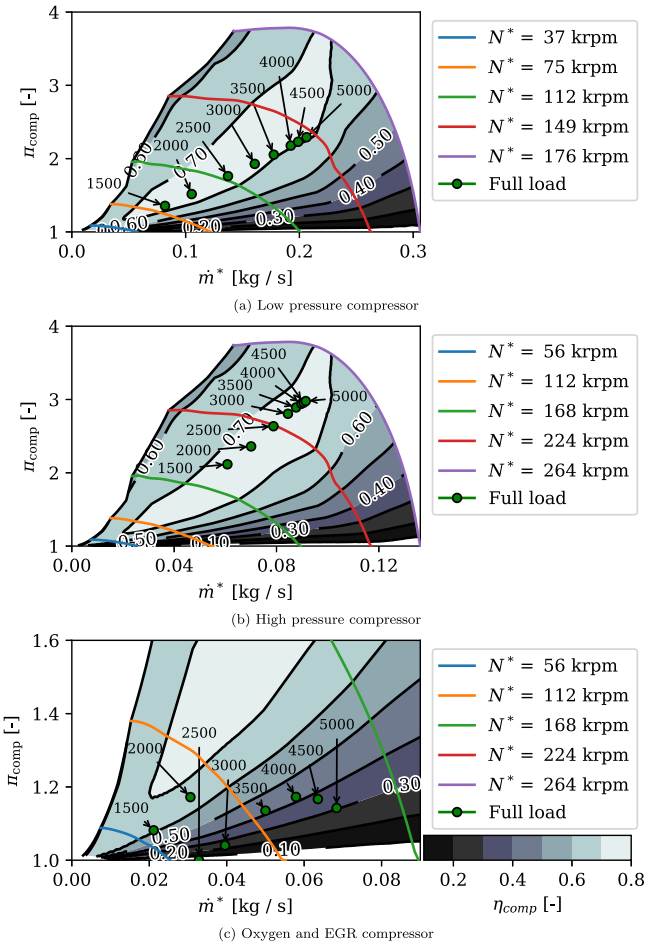

Fig. A.15. Compressor maps of the oxygen production cycle - CR20.

Appendix B. Combustion settings

The laws of combustion implemented in this paper follow the results obtained by Serrano et al. [24], where the authors implemented theoretical and experimental tools to study oxycombustion in a spark-ignition engine for different EGR and dilution conditions. In the mentioned study, an engine test bench is adapted to be supplied by O_2 and CO_2 pressurized tanks during the start-up. After the steady operation is achieved, the CO_2 supply is substituted by EGR. In addition, conventional operation with atmospheric air remains available in the facilities to obtain performance results and compare both working modes. The engine test bench layout is shown in Fig. B.16.

Different variables are measured, such as in-cylinder pressure, intake, exhaust pressure and temperature, emissions, and CO_2 concentration at intake. With in-cylinder pressure measurements, global parameters related to combustion as IMEP, combustion phasing and misfiring, maximum cylinder pressure, cycle-to-cycle variability, and heat release rate, using the thermodynamic combustion diagnosis tool CALMEC, which is an in-house software that has demonstrated validity for this type of calculations [44,45].

On the other hand, 0D-1D is implemented to estimate the thermochemical and fluid-dynamic behavior of oxycombustion at different dilution conditions. These tools are implemented to reduce the experimental test campaigns, determining theoretical limits regarding combustion stability, exhaust temperatures, and indicated efficiency.

The 0D modeling for thermo-chemical processes helps to determine auto-ignition delay, laminar flame speed, and flame temperature for different mixtures and thermodynamic conditions. This model uses the chemical kinetic mechanism proposed by Liu et al. [46] based on primary reference fuel. On the other hand, 0D-1D simulations are used to compute the fluid-dynamic behavior of the engine working at oxycombustion, which is initially calibrated using experimental data shown by Serrano et al. [23].

Firstly, the oxygen and EGR dilution strategies are evaluated using 0D-1D thermochemical calculations. Different operation points are assessed, establishing limits in terms of the variables determined by the model. These limits can be seen in Fig. B.17. Due to the complexity of knocking, a 0D model is not accurate enough to determine its occurrence. However, determining knocking probability relative to conventional combustion is acceptable for setting operation boundaries. Therefore, a region delimited with values where the auto-ignition delay leads to a similar knocking propensity as conventional combustion is shown in Fig. B.17(a). On the other hand, a minimum laminar flame of 0.5 m/s is set, which was identified as the value that generates the longest combustion duration that ensures stable flame progression. Also, a maximum flame temperature of 3000 K is established as the limit to ensure engine integrity.

Given the latter, it was found that an operation with nearly stoichiometric combustion and EGR values between 65%–75% is feasible in a spark-ignition engine, considering that EGR dilution leads to a

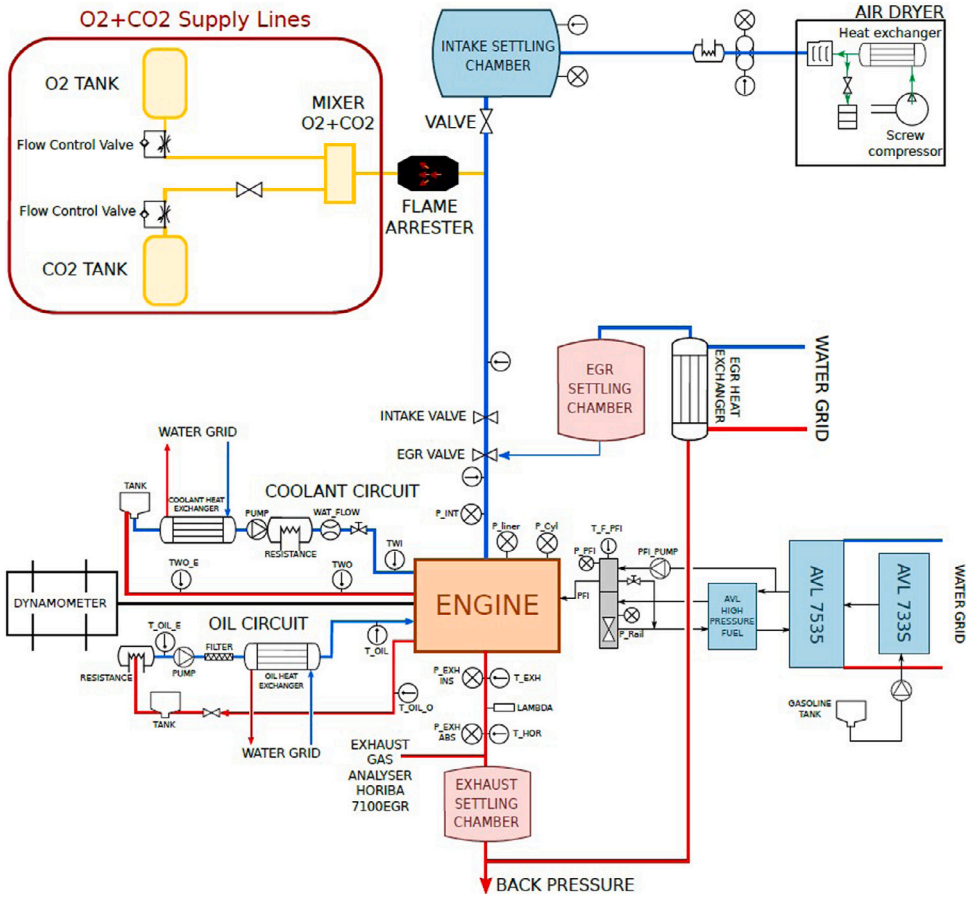

Fig. B.16. Engine test bench used by Serrano et al. [24] in their experiments.

lower oxygen mass rate requirement, demanding less energy for its production. Also, stoichiometric combustion allows an easier carbon dioxide separation from exhaust gases. This EGR range is validated in experimental conditions, where a maximum EGR of 73% can be reached while maintaining combustion stability and a minimum of 67% to guarantee exhaust gas temperatures that do not endanger the sensors and engine integrity. This experimental range demonstrates a reasonable agreement with the 0D-1D study and explains the current limits of EGR (and oxygen mass fraction as a consequence) and the use of stoichiometric combustion in the present paper.

On the other hand, different spark timings are studied experimentally in the EGR range established previously. This is performed to optimize the indicated efficiency for each EGR level and determine limits regarding knocking and combustion instability. Fig. B.18(a) and Fig. B.18(b) show IMEP variability and maximum amplitude of pressure oscillations, respectively, to determine combustion instabilities and knocking issues. It is seen that high EGR leads to combustion instabilities, as well as requiring advanced spark timings. Additionally, a low propensity for knocking is exhibited for the whole EGR range, being under a MAPO equal to 1, considered a safe threshold for knocking appearance. However, a lightly increasing as the spark timing is advanced in EGR values higher than 70%.

These results agree with those shown in Fig. B.17(a). An EGR of around 73% is near the combustion stability threshold, which produces high variability in the IMEP, risking the stable engine operation. On the other hand, Fig. B.18(b) shows with black stars the operation of conventional combustion at different spark timings. It is seen that the optimum operation of conventional combustion is above the MAPO limit established. This optimum conventional operation was also found near the region limited by the dashed line for knocking propensity exhibited in Fig. B.17(a). Additionally, the same figure shows that the region where oxy-fuel combustion is operated in this study is far from the knock propensity region (stoichiometric combustion and EGR between 67%–73%). This agrees with the considerable difference in MAPO between conventional combustion (around 5) and oxycombustion (under 1).

The explained experimental campaign was run using an IMEP of 1.1 MPa at 3000 rpm. For this reason, 0D-1D-CFD calculations are performed to determine the knocking propensity in a higher engine load (25 bar of IMEP) at the studied speed. First, consider 0D-1D fluid-dynamic calculations, where the spark timing is optimized at 70% EGR. Considering these optimum working conditions, a CFD calculation is performed to check for knocking presence during the combustion. The study indicates that knocking is not expected during high-load operation, where no considerable oscillations were found in the heat released rate. This opens room for an increase in the engine compression ratio to improve the engine performance.

Considering this explanation, a reduced model of premixed combustion is developed, where feasible ranges of spark timing and EGR are considered according to the commented results. Table B.15 shows the

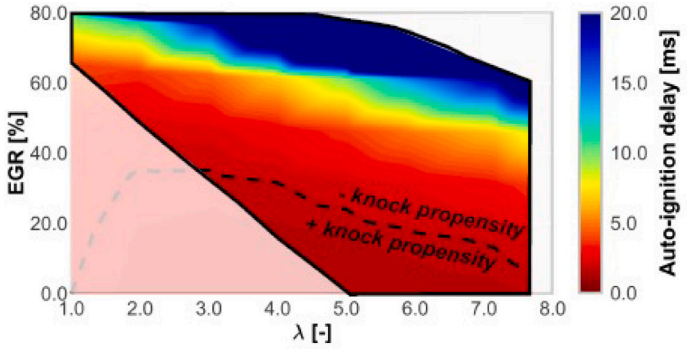

(a) Knocking propensity for different EGR and dilution levels. Results from Serrano et al. [24]

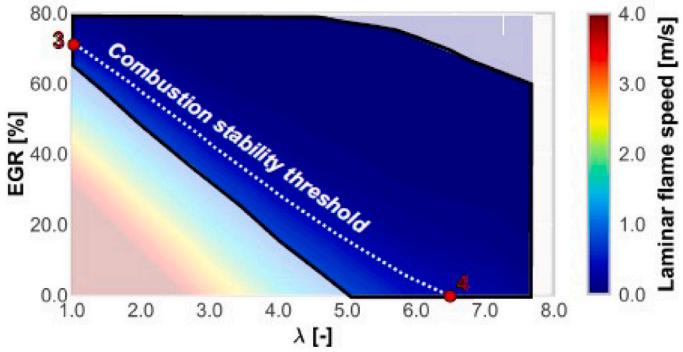

(b) Combustion stability for different EGR and dilution levels. Results from Serrano et al. [24]

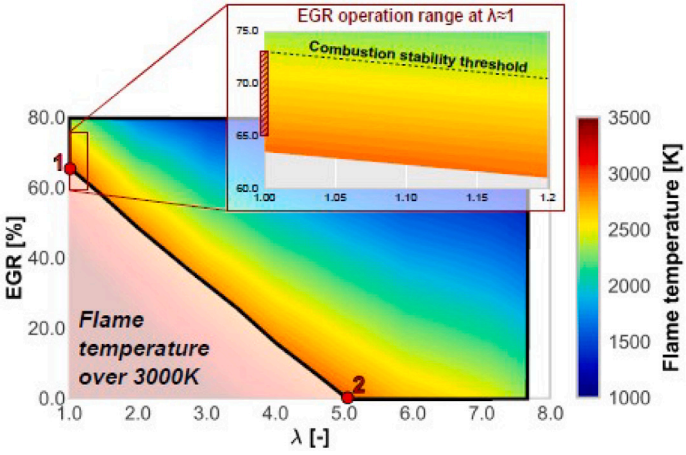

(c) Maximum flame temperature for different EGR and dilution levels. Results from Serrano et al. [24]

Fig. B.17. Analysis of chemical simulations for different EGR and dilution levels. Results from Serrano et al. [24].

Table B.15
Spark timing ranges used for optimizations in the present paper.

O_2 mass fraction	Maximum ST advance (°)	Minimum ST advance (°)
28%	−40	−30
30%	−35	−20
32%	−20	−11

used ranges for each EGR value studied in the present paper, in which the fuel consumption optimizations are performed in the present paper.

Using the in-house tool CALMEC, the heat release rate is determined for each studied case, determining the combustion duration, shape form, and ignition delay (to calculate the start of combustion). Using this information, correlations are developed to obtain these variables, depending on the EGR and spark timing. These correlations feed a Wiebe-type function in VEMOD, the in-house software used to simulate the studied cycle in the present paper, to impose a heat release rate for each studied case.

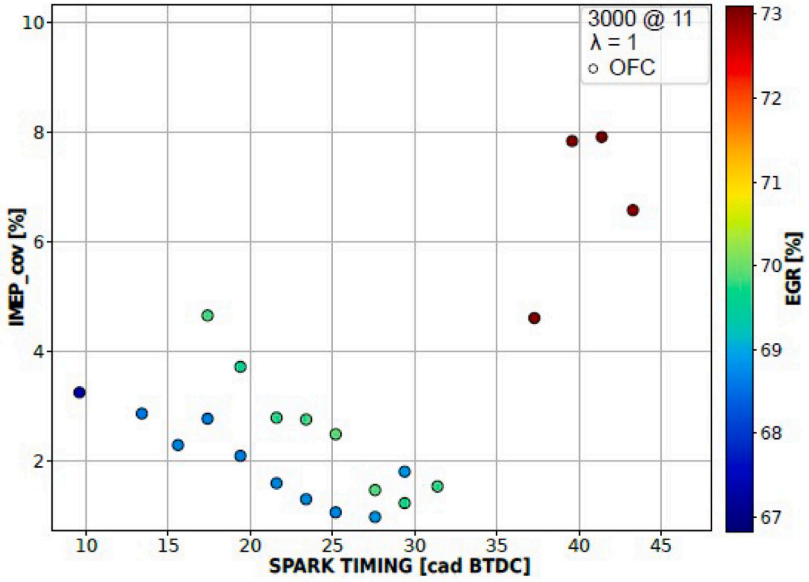

(a) IMEP variability at different EGR and spark timings. Results from Serrano et al. [24]

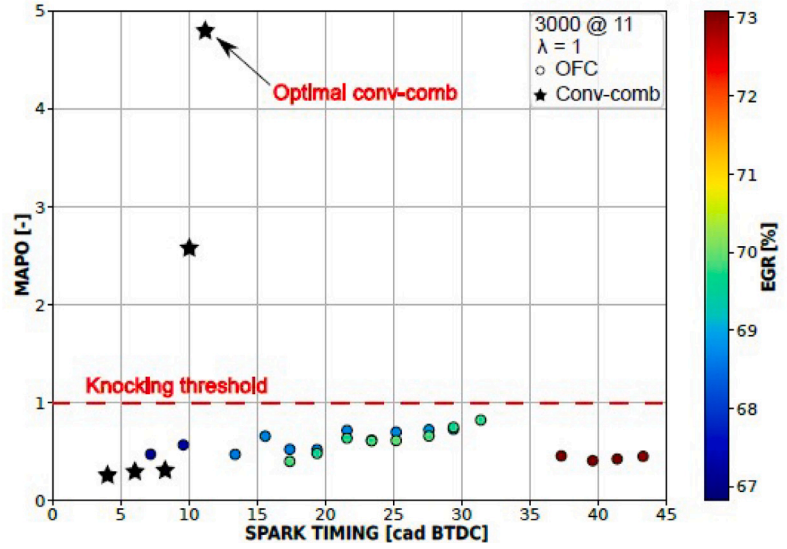

(b) Maximum amplitude of pressure oscillations at different EGR and spark timings. Results from Serrano et al. [24]

Fig. B.18. Indicators to determine combustion instabilities and knocking. Results from Serrano et al. [24].

References

[1] European Union. 2030 Climate & energy framework. 2021.
[2] European Union. Paris agreement. 2016.
[3] Habib MA, Nemitallah M, Ben-Mansour R. Recent development in oxy-combustion technology and its applications to gas turbine combustors and ITM reactors. Energy Fuels 2013;27(1):2–19.
[4] Zheng C, Liu Z. Oxy-fuel combustion fundamentals, theory and practice. Academic Press; 2018.
[5] Wu Z, Yu X, Fu L-Z, Deng J, Hu Z, Li L-G. A high efficiency oxyfuel internal combustion engine cycle with water direct injection for waste heat recovery. Energy 2014;70(1):110–20.
[6] Kang Z, Wu Z, Zhang Z, Deng J, Hu Z, Li L. Study of the combustion characteristics of a HCCI engine coupled with oxy-fuel combustion mode. SAE Int J Eng 2017;10:908–16.
[7] European Union. Commission proposes new Euro 7 standards to reduce pollutant emissions from vehicles and improve air quality. 2022.
[8] Tan Q, Hu Y. A study on the combustion and emission performance of diesel engines under different proportions of O_2&N_2 & CO_2. Appl Therm Eng 2016;108:508–15.
[9] Van Blarigan A, Kozarac D, Seiser R, Cattolica R, Chen J-Y, Dibble R. Experimental study of methane fuel oxycombustion in a spark-ignited engine. J Energy Resour Technol 2014;136:3.
[10] Mobasheri R, Aitouche A, Peng Z, Li X. A numerical study of the effects of oxy-fuel combustion under homogeneous charge compression ignition regime. Int J Engine Res 2021;23:649–60.
[11] Yu X, Wu Z, Fu L, Deng J, Hu Z, Li L. Study of combustion characteristics of a quasi internal combustion Rankine cycle engine. In: SAE/KSAE 2013 international powertrains, fuels & lubricants meeting 2013-01-2698. Society of Automotive Engineers; 2013.
[12] Wu Z, Fu L, Gao Y, Yu X, Deng J, Li L. Thermal efficiency boundary analysis of an internal combustion Rankine cycle engine. Energy 2016;94:38–49.
[13] Gao Y, Li L, Yu X, Deng J, Wu Z. Effect of compression ratio on internal combustion Rankine cycle based on simulations. In: Proceedings of SAE-China congress 2014: selected papers, vol. 328. 2015, p. 129–38.
[14] Wu H-W, Wang R-H, Chen Y-C, Ou D-J, Chen T-Y. Influence of port-inducted ethanol or gasoline on combustion and emission of a closed cycle diesel engine. Energy 2014;64:259–67.
[15] Wu F, Argyle MD, Dellenback PA, Fan M. Progress in O_2 separation for oxy-fuel combustion–A promising way for cost-effective CO_2 capture: A review. Prog Energy Combust Sci 2018;67:188–205.
[16] Zhu X, Yang W. Mixed conducting ceramic membranes fundamentals, materials and applications. Springer; 2017.
[17] Castillo R. Thermodynamic analysis of a hard coal oxyfuel power plant with high temperature three-end membrane for air separation. Appl Energy 2011;88(5):1480–93.

[18] Skorek-Osikowska A, Łukasz Bartela, Kotowicz J. A comparative thermodynamic, economic and risk analysis concerning implementation of oxy-combustion power plants integrated with cryogenic and hybrid air separation units. Energy Convers Manage 2015;92:421–30.
[19] Portillo E, Gallego Fernandez LM, Vega F, Alonso-Farinas B, Navarrete B. Oxygen transport membrane unit applied to oxy-combustion coal power plants: A thermodynamic assessment. J Environ Chem Eng 2021;9.
[20] Serrano J, Arnau F, a Cuevas LGarcí, Farias V. Oxy-fuel combustion feasibility of compression ignition engines using oxygen separation membranes for enabling carbon dioxide capture. Energy Convers Manage 2021;247.
[21] Arnau F, Novella R, García-Cuevas LM, Gutiérrez F. Adapting an internal combustion engine to oxy-fuel combustion with in-situ oxygen production. In: ASME 2021 internal combustion engine division fall technical conference. 2021.
[22] Arnau FJ, Benajes JV, Catalán D, Desantes JM, García-Cuevas LM, Serra JM, Serrano JR. Internal combustion engine and operating method of the same. Motor De Combustión Interna Y Método De Funcionamiento Del Mismo. p201930285, 28.03.2019. wo2020/193833a1. 2021.
[23] Serrano JR, Martín J, Gómez-Soriano J, Raggi R. Theoretical evaluation of the spark-ignition premixed oxyfuel combustion concept for future CO_2 captive powerplants. Energy Convers Manage 2021;244.
[24] Serrano JR, Martín J, Gómez-Soriano J, Raggi R. Exploring the oxy-fuel combustion in spark-ignition engines for future clean powerplants. In: Proceedings of the ASME 2022 ICEF, vol. 2022. 2022.
[25] Martin J, Arnau F, Piqueras P, Auñón A. Development of an integrated virtual engine model to simulate new standard testing cycles. In: WCX world congress experience. SAE International; 2018, 2018.
[26] Serrano J, Piqueras P, Morena JDeLa, Gómez-Vilanova A, Guilain S. Methodological analysis of variable geometry turbine technology impact on the performance of highly downsized spark-ignition engines. Energy 2021;215.
[27] Olmeda P, Martin J, Arnau F, Artham S. Analysis of the energy balance during world harmonized light vehicles test cycle in warmed and cold conditions using a virtual engine. Int J Engine Res 2019;21:1037–54.
[28] Arnau F, Martin J, Piqueras P, Auñon A. Effect of the exhaust thermal insulation on the engine efficiency and the exhaust temperature under transient conditions. Int J Engine Res 2021;22:2869–83.
[29] Serrano J, Arnau F, Dolz V, Tiseira A, Cervelló C. A model of turbocharger radial turbines appropriate to be used in zero- and one-dimensional gas dynamics codes for internal combustion engines modelling. Energy Convers Manage 2008;49(12):3729–45.
[30] Payri F, Serrano J, Fajardo P, Reyes-Belmonte M, Gozalbo-Belles R. A physically based methodology to extrapolate performance maps of radial turbines. Energy Convers Manage 2012;55:149–63.
[31] Galindo J, Navarro R, García-Cuevas LM, Tarí D, Tartoussi H, Guilain S. A zonal approach for estimating pressure ratio at compressor extreme off-design conditions. Int J Engine Res 2019;20(4):393–404.
[32] Galindo J, Tiseira A, Navarro R, Tarí D, Tartoussi H, Guilain S. Compressor efficiency extrapolation for 0D-1D engine simulations. In: SAE 2016 world congress and exhibition. SAE International; 2016, 2016-01-0554.
[33] Serrano JR, Olmeda P, Tiseira A, García-Cuevas LM, Lefebvre A. Theoretical and experimental study of mechanical losses in automotive turbochargers. Energy 2013;55:888–98.
[34] Serrano JR, Olmeda P, Arnau FJ, Reyes-Belmonte MA, Tartoussi H. A study on the internal convection in small turbochargers, proposal of heat transfer convective coefficients. Appl Therm Eng 2015;89:587–99.
[35] Serrano J, Olmeda P, Arnau F, Dombrovsky A. General procedure for the determination of heat transfer properties in small automotive turbochargers. SAE Int J Engines 2015;8(1):30–41.
[36] Serrano JR, Olmeda P, Arnau FJ, Dombrovsky A, Smith L. Methodology to characterize heat transfer phenomena in small automotive turbochargers: Experiments and modelling based analysis. In: Proceedings of the ASME turbo expo 2014: turbine technical conference and exposition, volume 1B. Marine; Microturbines, Turbochargers and Small Turbomachines; Steam Turbines: ASME.; 2014, Paper No: GT2014-25179.
[37] Catalán-Martínez D, Santafé-Moros A, Gozálvez-Zafrilla J, García-Fayos J, Serra J. Characterization of oxygen transport phenomena on BSCF membranes assisted by fluid dynamic simulations including surface exchange. Chem Eng J 2020;387:124069.
[38] Komninos N, Rogdakis E. Design considerations for an Ericsson engine equipped with high-performance gas-to-gas compact heat exchanger: A numerical study. Appl Therm Eng 2018;133:749–63.
[39] Li X, Peng Z, Pei Y, Ajmal T, Rana K-J, Aitouche A, et al. Oxy-fuel combustion for carbon capture and storage in internal combustion engines – A review. Int J Energy Res 2021;46:505–22.
[40] Li X, Pei Y, Ajmal T, Rana K, Aitouche A, Mobasheri R, et al. Numerical investigation on implementing Oxy-Fuel Combustion (OFC) in an ethanol-gasoline Dual-Fuel Spark Ignition (DFSI) engine. Fuel 2021;302:121162.
[41] Ditaranto M, Hals J. Combustion instabilities in sudden expansion oxy–fuel flames. Combust Flame 2006;146:493–512.
[42] Mohammed A, Elkhazraji A, Jan S, Johansson B. Study on the performance and emissions of HCCI oxy-fuel combustion in a CFR engine with recirculated carbon dioxide. SAE Technical Paper 2020-01-2065, 2020.
[43] Arnau FJ, Bracho G, García-Cuevas LM, Farias VH. A strategy to extend load operation map range in oxy-fuel compression ignition engines with oxygen separation membranes. Appl Therm Eng 2023;226:120268.
[44] Payri F, Olmedo P, Martin J, Carreño R. A new tool to perform global energy balances in di diesel engines. SAE Int J Eng 2014;7:43–59.
[45] Benajes J, Olmeda P, Martín J, Carreño R. A new methodology for uncertainties characterization in combustion diagnosis and thermodynamic modelling. Appl Therm Eng 2014;71:389–99.
[46] Liu Y-D, Jia M, Xie M-Z, Pang B. Enhancement on a skeletal kinetic model for primary reference fuel oxidation by using a semidecoupling methodology. Energy Fuels 2012;26:7069–83.